nature communications

Article

https://doi.org/10.1038/s41467-025-62558-4

PROCR diminishes the efficacy of radiation by impairing T-cell-mediated antitumour immunity

Received: 30 October 2023

Accepted: 22 July 2025

Published online: 04 August 2025

Check for updates

Weipeng Chen[1,2,6], Chuqing Zhang[1,3,6], Zhe Li[1,3,6], Zhimin Xu[1,3], Cong Ding[1,4], Jiawei Wu[1,5], Hanmiao Wei[1,3], Zhenji Deng[1,3], Tingxiang He[1,3], Liufen Long[1], Yanping Mao[1,3] ✉, Jun Ma[1,3] ✉ & Xiaoyu Liang[1,3] ✉

T cell dependent anti-tumour immunity reprogrammed by radiotherapy is critical for its efficacy. However, the mechanisms by which tumour cells hinder this process remain poorly understood. Here, we show that tumour cells expressing protein C receptor (PROCR) dampen antitumour immunity by promoting the production of interleukin-6 (IL-6), which inhibits the differentiation of T helper 1 (Th1) cells and suppresses the function of $CD8^+$ T cells. We also demonstrate that radiation therapy enhances PROCR expression by reducing its selective autophagic degradation through the modulation of p62 phosphorylation, a process governed by mTORC1 signalling. This suggests that PROCR upregulation is an intrinsic cellular response to radiation. Targeting PROCR or IL-6 improves the efficacy of radiotherapy in preclinical models, including humanized mice and immunocompetent mice. In patients with nasopharyngeal carcinoma, higher PROCR expression correlates with reduced Th1 cell infiltration and worse functional state of $CD8^+$ T cells. Meanwhile, elevated levels of PROCR or IL-6 are associated with reduced responsiveness to radiotherapy. These findings identify PROCR as a key immunosuppressive factor linked to radiotherapy resistance and highlight its potential as a therapeutic target to enhance treatment outcomes.

Nearly half of cancer patients will receive radiotherapy as part of their comprehensive treatment[1]. The efficacy of irradiation depends in part on the direct cytotoxic effects of DNA damage on tumours and stroma and in part on innate and adaptive immune responses[2–4]. For decades, research into improving radiotherapy outcomes has focused mainly on the cancer cell itself, without knowledge of the complex biological interactions between tumour and the tumour immune microenvironment (TIME). The recent discovery that DNA damage induced by radiation in tumour cells can activate intracellular nucleic acid sensors and inflame the TIME transformed our understanding of the mechanistic basis of radiotherapy[5–7]. The type-I interferon signalling triggered by cytoplasmic DNA-sensing cyclic GMP–AMP synthase (cGAS)–stimulator of interferon genes (STING) pathway appears to be phenotypically dominant in this process[7–9]. This signalling mainly works by recruiting and assisting tumour-specific T cells to kill tumour cells. More importantly, in a variety of tumours, such as rectal cancer

[1]State Key Laboratory of Oncology in South China, Collaborative Innovation Center of Cancer Medicine, Guangdong Key Laboratory of Nasopharyngeal Carcinoma Diagnosis and Therapy, Guangdong Provincial Clinical Research Center for Cancer, Sun Yat-sen University Cancer Center, Guangzhou, PR China. [2]Department of Nuclear Medicine, Sun Yat-Sen University Cancer Center, Guangzhou, PR China. [3]Department of Radiation Oncology, Sun Yat-sen University Cancer Center, Guangzhou, PR China. [4]Department of Ultrasound and Electrocardiogram, Sun Yat-Sen University Cancer Center, Guangzhou, PR China. [5]Department of Pathology, Sun Yat-Sen University Cancer Center, Guangzhou, PR China. [6]These authors contributed equally: Weipeng Chen, Chuqing Zhang, Zhe Li. ✉e-mail: maoyp@sysucc.org.cn; majun2@mail.sysu.edu.cn; liangxy1@sysucc.org.cn

or non-small-cell lung cancer (NSCLC)[10,11], it is found that the efficacy of radiotherapy is closely related to whether anti-tumour T cell-related immunity can be effectively reshaped. However, oxidative stress, as the main effect of radiotherapy[12], not only causes DNA breakage[13] and activates the cGAS-STING pathway[14], but also has other complex biological effects[15]. Therefore, in reality, the net effects of radiotherapy on immune remodelling show contradictory characteristics, that is, completely contradictory conclusions are drawn in different specific cases. Especially considering that most patients do not have inactivating mutations in the cGAS-STING pathway. Therefore, it is of great significance to further elucidate and explore the inherent downstream regulatory patterns and key pathways of radiotherapy-related oxidative stress to control the direction of radiotherapy immune remodelling.

Cancer stem-like cells (CSCs) are considered an important factor contributing to radioresistance[16]. More importantly, cancer stem cells are more resistant to various stress. Compared with differentiated tumour cells, cancer stem cells equip with unique pathways to resist[17]. Protein C receptor (PROCR), originally identified as an endothelial cell-specific transmembrane glycoprotein, has recently emerged as a cancer stem cell marker in different types of cancer[18,19]. In breast cancer patients, this molecule can be used as a biomarker to stratify triple-negative breast cancer into clinically relevant subgroups and may provide a promising treatment target[18]. In nasopharyngeal carcinoma (NPC), PROCR maintains nasopharyngeal cancer cell stemness via lipid metabolic regulation and mitochondrial fission[19]. However, whether PROCR expression in tumours is involved in oxidative stress and immune remodelling after radiotherapy remains to be further explored.

In this work, we show that PROCR functions as an immunosuppressive factor that promotes radioresistance by driving interleukin-6 secretion, inhibiting Th1 cell differentiation, and impairing $CD8^+$ T-cell function. We demonstrate that radiotherapy-induced activation of mTORC1 prevents the selective autophagic degradation of PROCR mediated by p62. Targeting PROCR or IL-6 enhances radiotherapy efficacy in preclinical tumour models. These findings collectively provide valuable understanding of the intricate dynamics of the immune response to radiotherapy and identify potential therapeutic targets for improving cancer treatment.

Results

PROCR dampens the efficacy of radiotherapy in an immune-dependent manner

We previously found that PROCR could sustain tumour stemness by reprogramming lipid metabolism[19]. Given that both cancer stem cells and lipid metabolism are involved in determining sensitivity to radiotherapy[20–22], we further explored the role of PROCR on radiotherapy. Considering that PROCR is also expressed on the endothelial cells, by performing two-colour immunohistochemical staining for PROCR and CD31 in NPC specimens, we extracted the tumour fraction, analysed the expression levels of PROCR, and stratified the patients according to the expression levels of PROCR in the tumour bed (22 tumours with local regional relapse and their paired counterparts from SYSUCC NPC cohort) (Fig. 1A). It was found that significantly lower expression of PROCR in relapse-free patients than in locoregionally relapsed patients after radiotherapy (Fig. 1B). However, in in-vitro cellular models, we observed that knocking out *PROCR* in the NPC cell lines HONE1 or SUNE-1 (Supplementary Fig. 1A) did not affect cellular DNA double-strand breaks nor cell death after irradiation (Supplementary Fig. 1B, C). Moreover, cells with PROCR deficiency showed no differences in cell proliferation compared with wild-type cells (Supplementary Fig. 1D). Notably, although PROCR did not directly affect cell death after irradiation under in-vitro conditions, we found that irradiation can upregulate the expression of PROCR in multiple cell lines (Supplementary Fig. 1E).

The efficacy of radiotherapy depends not only on the tumour cells themselves but is also highly influenced by the tumour microenvironment[23,24]. Therefore, we further explored whether PROCR affected radiotherapy efficacy by modulating the immune microenvironment. To this end, we started by using a heterotopic transplantation model based on the murine MC38 cell line, which is a preclinical model widely used to evaluate host antitumour immunity, including that after irradiation. Consistent with NPC cell lines, *PROCR* knockout MC38 cells also showed no differences in in-vitro cell proliferation compared with wild-type cells (Supplementary Fig. 1F, G). However, these *PROCR* knockout MC38 cells formed smaller tumours when inoculated subcutaneously into C57BL/6 mice (Fig. 1C). More importantly, such in vivo tumour growth inhibition led by *PROCR* knockout was T-cell immunity dependent (Supplementary Fig. 1H). To exclude the confounding effect of PROCR on tumour size of baseline level, we further established inducible *PROCR* knockdown MC38 cell lines based on a doxycycline (Dox)-inducible shRNA expression system ($MC38^{Tet\text{-}sh\mathit{PROCR}}$) (Supplementary Fig. 1I). After subcutaneous inoculation of $MC38^{Tet\text{-}sh\mathit{PROCR}}$ cells, mice received irradiation and doxycycline gavage. The knockdown efficiency of *PROCR* was confirmed in vivo (Supplementary Fig. 1J); as expected, we found that silencing *PROCR* led to a better curative effect of irradiation (Fig. 1D-F). Moreover, consistent with previous results, after T cell depletion, the tumour-controlling effects induced by suppression of PROCR disappeared, under the conditions with or without irradiation (Fig. 1G-I). More convincingly, *PROCR*-KO MC38 cells also showed no significant differences in tumour volumes compared with wild-type cells in conditions with or without irradiation after inoculation in T cell immunity deficient BALB/c nude mice (Fig. 1J, K). To validate the potential of PROCR as a radiotherapy sensitization target, we injected neutralizing antibodies against murine PROCR combined with irradiation and found that irradiation-mediated antitumour effect was significantly enhanced (Fig. 1L, M). A prior study indicated that PROCR was upregulated in exhausted $CD8^+$ T cells; however, we observed that PROCR blockade had no significant effects in PROCR-deficient MC38 models (Supplementary Fig. 1K-M), further confirming that PROCR blockade exerts its effects by directly targeting tumour cells. Together, these data suggested that PROCR has the potential to be an effective target for radiotherapy sensitization. On one hand, PROCR could be induced by irradiation, on the other hand, blockade of PROCR enhanced the efficacy of radiotherapy in a T-cell immunity-dependent manner.

PROCR blockade potentiates antitumour immunity by promoting Th1 differentiation and $CD8^+$ T cell function

Next, we sought to explore the mechanism by which PROCR affected the T cell dependent anti-tumour immunity. In fresh tumour tissues collected from NPC patients, we found that the expression levels of PROCR on tumour cells were negatively correlated with the proportion of Th1 cells or the expression levels of key effector molecules (IFN-γ, granzyme B and perforin) of $CD8^+$ T cells (Fig. 2A–D, Supplementary Fig. 2A, B). Therefore, we speculated that PROCR was involved in inhibiting Th1 differentiation and suppressing $CD8^+$ T cell function, while in the context of radiotherapy, this effect was exacerbated due to its further upregulation. To verify this hypothesis, we isolated $CD4^+$ or $CD8^+$ T cells from fresh NPC tumour tissues, activated them with low-dose CD3 antibodies, and cocultured them with HONE1 cells with or without *PROCR* knockout. As expected, we found that co-culturing with *PROCR* knockout tumour cells led to enhanced Th1 differentiation in $CD4^+$ T cells and higher effector molecules expression in $CD8^+$ T cells; moreover, after irradiation, T cells co-cultured with wild-type HONE1 cells showed further decreased levels of IFN-γ, granzyme B or perforin, while co-culturing with *PROCR* knockout cells did not show this effect (Fig. 2E-H). More importantly, we observed similar effects with the culture supernatant from irradiated or non-irradiated parental (sgGFP) and *PROCR*-KO (sg*PROCR*) HONE1 cells as in the above

https://doi.org/10.1038/s41467-025-62558-4

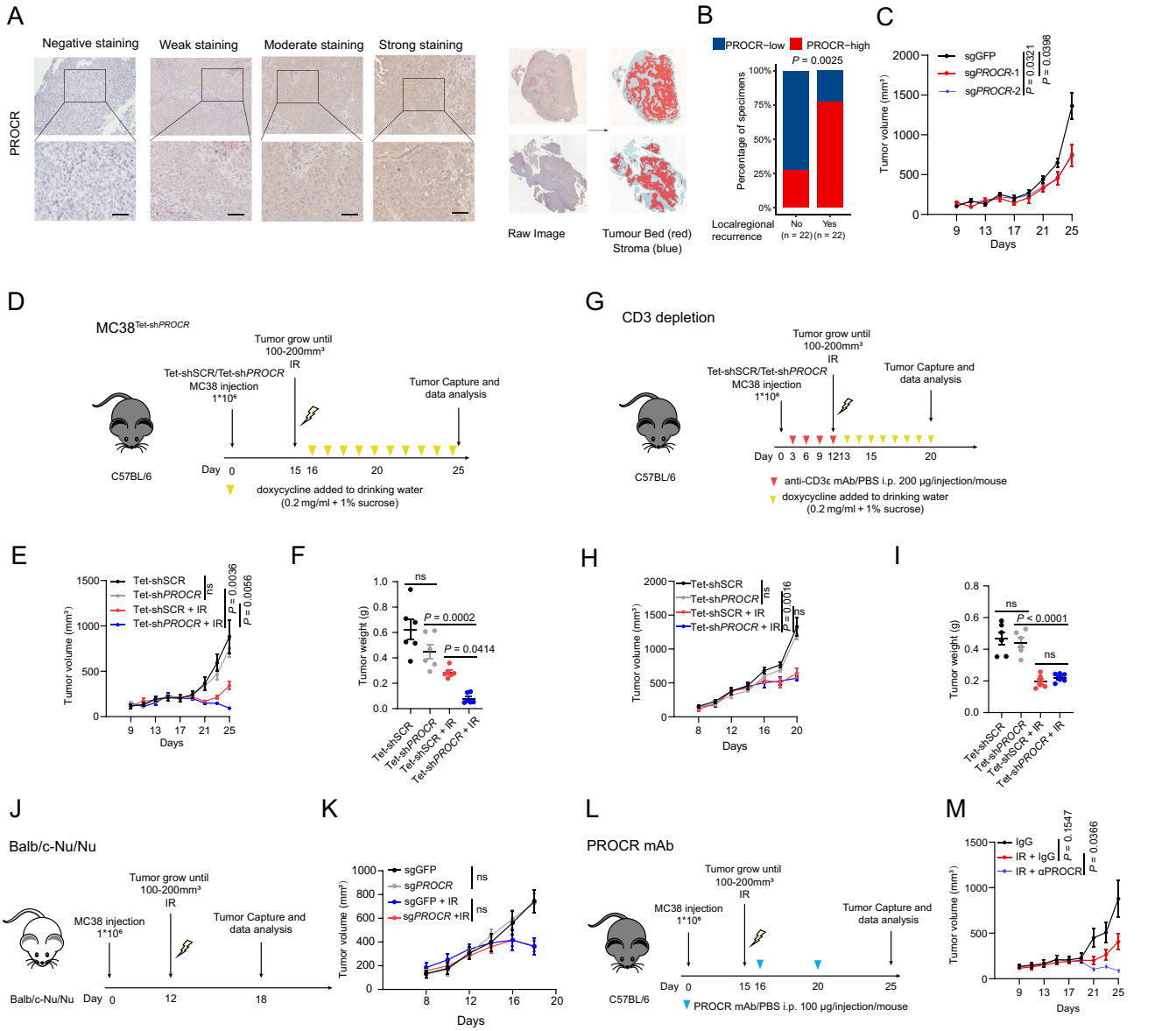

Fig. 1 | PROCR dampens the efficacy of radiotherapy via an immune-dependent way. A Left: representative images of dual IHC staining of paraffin-embedded human NPC tissue sections using PROCR (brown) and CD31(red). Scale bar, 50 μm. Right: separation of tumour and stroma areas using the HALO software. **B** Correlation analysis of PROCR expression and locoregional recurrence status after radical chemoradiotherapy. The *P* value was determined by two-tailed χ^2 test. **C** PROCR knockout (sg*PROCR*) or parental (sgGFP) MC38 cells were inoculated into C57BL/6 mice (1×10^6 MC38 cells/mouse) to construct xenograft growth models. Tumour volume for each group were shown (6 mice per group). **D**–**F** MC38 cells expressing inducible shScramble (Tet-shSCR) or inducible sh*PROCR* (Tet-sh*PROCR*) were inoculated subcutaneously into C57BL/6 mice (1×10^6 MC38 cells/mouse, 6 mice per group). 15 days after inoculation, doxycycline (0.2 mg/ml + 1% sucrose) was added to drinking water. Mice in the IR-treated groups were subjected to focal radiation with a single fraction of 4 Gy on day 15 after tumour cell inoculation. Tumour growth curves were monitored, and tumour volumes and weights were compared at the indicated time points. **G**–**I** Tet-shSCR or Tet-sh*PROCR* MC38 cells were inoculated (6 mice per group). Overall T cells were depleted with anti-CD3ε mAb at indicated time points. Doxycycline was added to drinking water as indicated. Mice in the IR-treated groups were subjected to 4 Gy radiation. Tumour growth curves were monitored, and tumour volumes and weights were compared at the indicated time points. **J**, **K** sg*PROCR* or sgGFP MC38 cells were inoculated into Balb/c-Nu/Nu mice (5 mice per group). Mice in the IR-treated groups were subjected to 4 Gy radiation. Tumour growth curves were monitored and compared at the indicated time points. **L**, **M** MC38 cells were inoculated into C57BL/6 mice (6 mice per group). 15 days after inoculation, mice were treated with irradiation plus IgG or anti-PROCR monoclonal antibody. Tumour growth curves were monitored and compared at the indicated time points. Data are shown as mean ± SEM. *P* values were calculated using one-way ANOVA (**F**, **I**) or two-way ANOVA (**C**, **E**, **H**, **K**, **M**). Source data are provided as a Source Data file.

experiments (Fig. 2I–L). Consistently, murine CD4 or CD8 T cells cultured with supernatant from MC38 cells, with or without *PROCR* knockout, showed similar results to their human counterparts (Supplementary Fig. 2C–F). To further demonstrate the effect of PROCR on $CD8^+$ T cells, we assessed the efficacy of $CD8^+$ T cells in killing tumour cells. To better mimic tumour-specific killing, we constructed chimeric antigen receptor T cells (CAR-T) targeting ERBB2 in HONE1 cells, which express high levels of ERBB2 (Supplementary Fig. 2G). Consistent with previous results, HER-CAR-T cells showed enhanced killing efficacy when cultured with supernatant from *PROCR* knockout HONE1 cells compared to wild-type cells (Supplementary Fig. 2H, I).

To further validate these findings in vivo and better uniform with our patient data, we conducted ex vivo flow cytometric analysis of tumour-infiltrating T cells isolated from irradiated tumours formed by

https://doi.org/10.1038/s41467-025-62558-4

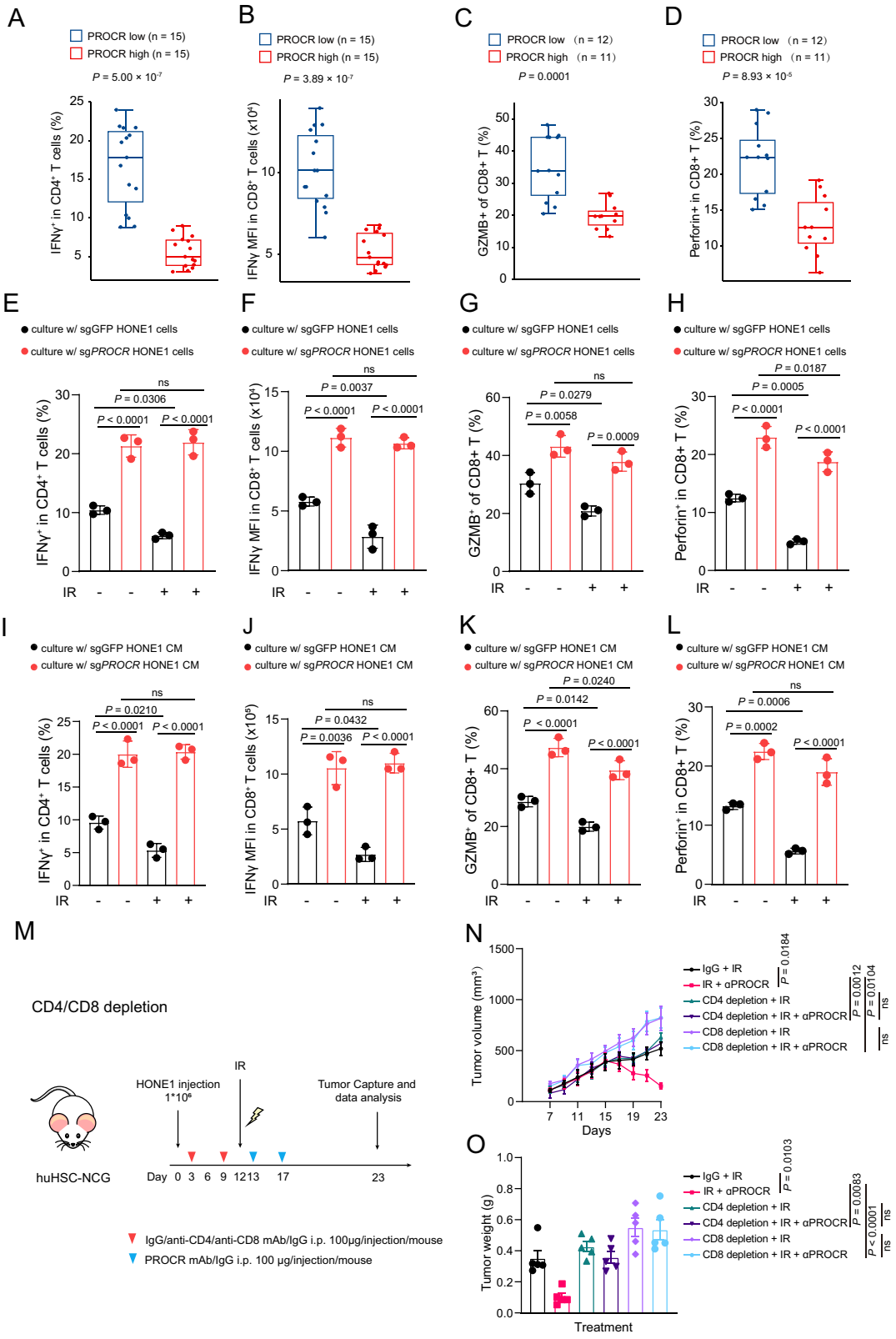

wild-type or *PROCR* knockout HONE1 cells in HuHSC-NCG humanized mice that reconstructed immune system. As expected, we found that *PROCR* knocking-out led to increased Th1 ratio as well as higher effector molecules expression in CD8⁺ T cells (Supplementary Fig. 2J-L). Furthermore, we used a neutralizing antibody against PROCR in huHSC-NCG mice bearing HONE1 tumours and found that co-administration of the antibody also promoted the efficacy of radiotherapy, showing further decreased tumour volumes (Fig. 2M-O). Meanwhile, the sensitizing effect of radiotherapy by PROCR neutralizing antibody was almost eliminated after using the neutralizing antibody to deplete human-derived CD4 or CD8 T cells (Fig. 2M-O). In the native immune system mouse model based on C57BL/6 mice and MC38 cells, after knocking out *PROCR* or addition of the PROCR neutralizing antibody, the tumour infiltrated Th1 cells ratio and CD8⁺

Fig. 2 | PROCR blockade potentiate anti-tumour immunity by promoting Th1 differentiation and CD8⁺ T cells function. Proportion of Th1 (**A**), IFNγ MFI of CD8⁺ T cells (**B**), proportion of GZMB⁺ cells (**C**) and perforin⁺ cells in CD8⁺ T cells (**D**) in independent human NPC specimens were evaluated by flow cytometry. PROCR high versus low was determined by the median value of mean fluorescence intensity (MFI) of $CD45^-EPCAM^+$ tumour cells. Sample sizes included 15 patients in the PROCR low group and 15 patients in the PROCR high group for (**A**, **B**); and 12 patients in the PROCR low group and 11 patients in the PROCR high group for (**C**, **D**). The boxplots in **A**–**D** indicate the median (centre), 25th, and 75th percentiles (box boundaries), and minimum and maximum (the whiskers). Proportion of Th1 cells (**E**) and IFNγ MFI of CD8⁺ T cells (**F**), proportion of GZMB⁺ cells (**G**) and perforin⁺ cells (**H**) in human NPC specimens after coculture with irradiated *PROCR*-knockout (sg*PROCR*) and parental (sgGFP) HONE1 cells. Proportion of Th1 cells (**I**) and IFNγ MFI of CD8⁺ T cells (**J**), proportion of GZMB⁺ cells (**K**) and perforin⁺ cells (**L**) in human NPC specimens after coculture with culture medium (CM) from irradiated *PROCR*-knockout (sg*PROCR*) and parental (sgGFP) HONE1 cells. **M**–**O** HONE1 cells were inoculated into huHSC-NCG mice (1×10^6 HONE1 cells/mouse, 5 mice per group). $CD4^+$ or $CD8^+$ T cells were depleted with anti-human CD4 or anti-human CD8 antibody, respectively. 12 days after inoculation, mice were treated with irradiation, with or without αPROCR. Tumour growth curves were monitored, and tumour volumes and weights were compared at the indicated time points. $n = 3$ independent experiments (**E**-**L**). Data are shown as mean ± SD (**E**–**L**) or mean ± SEM (**N**, **O**). *P* values were calculated using two-tailed unpaired t test (**A**–**D**), one-way ANOVA (**E**–**L**, **O**) or two-way ANOVA (**N**). Source data are provided as a Source Data file.

T cells function was significantly improved under radiotherapy (Supplementary Fig. 2M-P, Supplementary Fig. 2Q-T). Moreover, consistent with results from humanized mice model, we observed that in MC38 models, both CD4- and CD8-depleting antibodies abolished the irradiation-sensitizing efficacy of the PROCR antibody, although the effect of the CD8-depleting antibody was more prominent (Supplementary Fig. 2U-Z). Taken together, the above findings indicated that PROCR blockade could promote Th1 differentiation and enhance the function of $CD8^+$ T cells, thereby potentiating antitumour immunity.

PROCR promotes IL-6 secretion, leading to inhibition of anti-tumour immunity

We then sought to explore the mechanism by which PROCR suppressed T-cell dependent antitumour immunity. Our previous experiments suggested that PROCR affect the differentiation and function of T cells probably by changing components in the culture supernatant. Given that both tumour cells secreted metabolites and cytokines may exert immunosuppressive effects on T cells[25–27]; we used ultrafiltration tubes with a 3 kD filter membrane to process the supernatant from irradiated wild-type or *PROCR*-knockout HONE1 cells, allowing a basic separation of these two types of substance. We found that the supernatant retained on the 3 kD filter reproduced similar effects of the unprocessed supernatant, while the filtered liquid did not (Fig. 3A, B). Given that most cytokines have molecular weights greater than 3 kD, we speculated that effects related to *PROCR* knockout were associated with changes in cytokines in the supernatant.

Type I IFNs can be produced and secreted by tumour cells under stress and play an important role in modulating T-cell-dependent antitumour immunity in various conditions, including irradiation[24]. Therefore, we evaluated the impact of PROCR on type I IFNs production by detecting the phosphorylation levels of IRF3 and STAT1 and the expression levels of representative type I IFNs (IFNB1/IFNA4). However, knocking-out of *PROCR* showed no obvious effect on the phosphorylation levels of neither IRF3 nor STAT1, regardless of irradiation or under the stimulation of typical DAMPs or PAMPs (HT-DNA or 5'ppp-dsRNA) (Supplementary Fig. 3A). Consistently, the expression levels of both IFNB1 and IFNA4 were also similar between the WT and *PROCR*-KO cells under irradiation (Supplementary Fig. 3B). We next assessed other inflammation-related cytokines in the supernatant. By comparing the cytokine profiles, we found that the levels of IL-6 and IL-8 were changed most prominently after *PROCR* knockout (Fig. 3C). By enzyme-linked immunosorbent assays (ELISAs), we further confirmed the changes of these two cytokines (Fig. 3D). Then, we sought to clarify the role of these two cytokines by adding exogenous recombinant IL-6, or transfecting siRNA targeting *IL8*, and found that adding IL-6 could effectively reverse the effects of knocking-out *PROCR*, while silencing *IL8* did not produce any significant effects (Fig. 3E, F). More convincingly, when we pretreated T cells with an anti-IL-6R antibody, the effects induced by PROCR overexpression were abolished as well (Fig. 3G). Therefore, we speculated that PROCR mediated the immunosuppressive effects by upregulating IL-6. To verify this hypothesis, we re-expressed PROCR in PROCR-deficient HONE1 cells; as expected, the expression of *IL6* was upregulated (Fig. 3H); more importantly, the inhibitory effect of overexpression of PROCR on differentiation of Th1 cells and function of $CD8^+$ T cells was almost abolished when IL-6 was knocked down by transfection of siRNA. (Fig. 3I). In addition, we also explored whether IL-6 had a regulatory role on PROCR, especially under irradiation. However, by treating HONE1 cells with IL-6 under the condition with or without radiotherapy and we found that IL6 treatment did not show significant effect on PROCR expression (Supplementary Fig. 3C); on the other hand, we transfected siRNA targeting *IL6* into HONE1 cells before radiotherapy and found that knocking-down of *IL6* (Supplementary Fig. 3D) had no obvious effect on the upregulation of PROCR by radiotherapy either (Supplementary Fig. 3E). Finally, for murine cells, it was also confirmed that a similar regulatory relationship existed between PROCR and IL-6 in MC38 cells (Supplementary Fig. 3F) and that inhibition of IL-6 led to enhanced Th1 cells differentiation and upregulated IFNγ expression in $CD8^+$ T cells in vitro (Supplementary Fig. 3G).

To confirm the presence of the PROCR-IL-6 axis in vivo and its effect on the efficacy of radiotherapy, we conducted a series of experiments. First, in humanized mouse model with HONE1 xenografts, induction of PROCR expression significantly reduced radiotherapy efficacy which was consistent with previous data; whereas anti-IL-6R antibody not only counteracted the inhibitory effect of PROCR overexpression, but also further enhanced the antitumour efficacy of radiotherapy (Fig. 3J-L). Secondly, in MC38 cells based murine tumour model of native immune system, we also re-expressed PROCR in *PROCR*-KO MC38 cells in an inducible pattern (Supplementary Fig. 3H). In agreement with the humanized mice, PROCR overexpression resulted in larger tumour volumes under irradiation, which could also be reversed by adding anti-IL-6R (Supplementary Fig. 3I-K). Thirdly, we examined the effect of intratumour injection of IL-6 on MC38 tumours treated with irradiation combined with anti-PROCR antibody; and found that injection of IL-6 counteracted the radiosensitizing effect of PROCR blockade (Supplementary Fig. 3L-N). Additionally, in vitro experiments revealed that IL-6 treatment did not influence the cell death of irradiated tumour cells (Supplementary Fig. 3O). More importantly, when T cells were depleted via CD3 antibody, the effect of anti-IL6R treatment in decreasing tumour volumes or the effect of IL-6 in promoting tumour volumes were abolished (Supplementary Fig. 3P-U), highlighting the influence of IL-6 signalling on regulating T-cell dependent antitumour immunity.

PROCR induces p65 activation via RSK1 to promote IL-6 transcription

Next, we investigated the mechanism by which PROCR upregulated IL-6. To this end, we performed RNA sequencing on irradiated HONE1 cells with or without *PROCR* knockout. Through gene set enrichment analysis (GSEA), we identified several signalling pathways with the most prominent enrichment when *PROCR* was present; notably, the enrichment of the nuclear factor kappa-light-chain-enhancer

https://doi.org/10.1038/s41467-025-62558-4

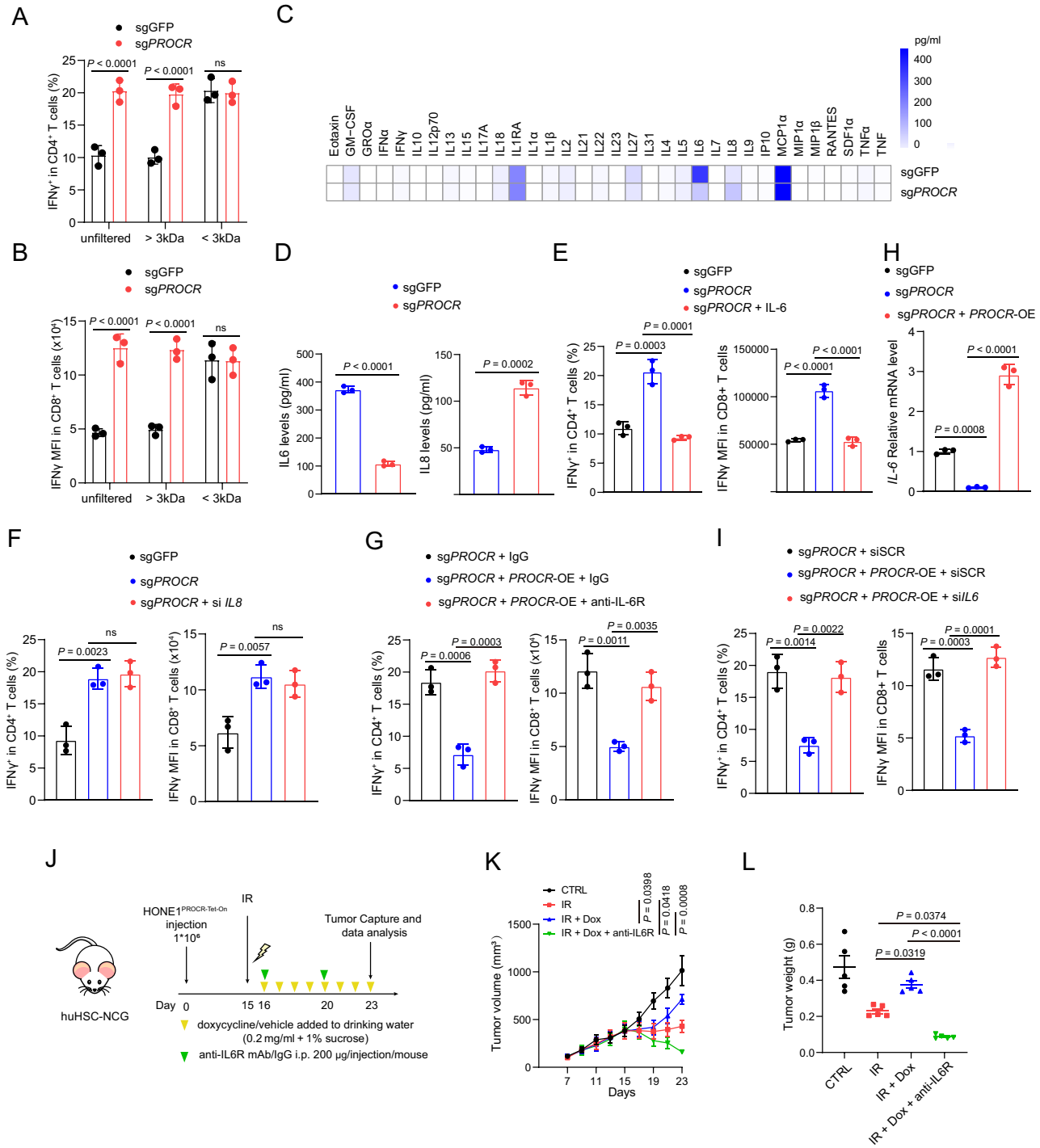

Fig. 3 | PROCR promotes IL6 secretion leading to inhibition of anti-tumour immunity. Proportion of Th1 cells (**A**) and IFNγ MFI of $CD8^+$ T cells (**B**) in human NPC specimens after coculture with indicated culture medium (CM). **C** Multiplex cytokine array showing cytokine production in CM of *PROCR*-knockout (sg*PROCR*) and parental (sgGFP) HONE1 cells. **D** ELISA for IL-6 and IL-8 in the supernatant of sgGFP and sg*PROCR* HONE1 cell. **E** Proportion of Th1 cells and IFNγ MFI of $CD8^+$ T cells in human NPC specimens after coculture with CM from sg*PROCR* and sgGFP HONE1 cells, with or without anti-IL-6 mAb. **F** Proportion of Th1 cells and IFNγ MFI of $CD8^+$ T cells in human NPC specimens after coculture with CM from sg*PROCR* and sgGFP HONE1 cells, with or without *IL8* knockdown. **G** Proportion of Th1 cells and IFNγ MFI of $CD8^+$ T cells in human NPC specimens after coculture with HONE1 sg*PROCR* CM + IgG, PROCR-rescue (sg*PROCR* + *PROCR*-OE) CM + IgG, or PROCR-rescue CM + anti-IL-6R antibody. **H** Quantitative polymerase chain reaction (qPCR) analysis of *IL6* expression in parental sgGFP, sg*PROCR*, and PROCR-rescue HONE1 cells. **I** Proportion of Th1 cells and IFNγ MFI of $CD8^+$ T cells in human NPC specimens after coculture with HONE1 *PROCR*-knockout (sg*PROCR* + siSCR) CM, PROCR-rescue (sg*PROCR* + *PROCR*-OE + siSCR) CM, or PROCR-rescue with *IL6* knockdown (sg*PROCR* + *PROCR*-OE + si*IL6*) CM. **J**–**L** $HONE1^{PROCR\text{-}Tet\text{-}On}$ cells were inoculated into huHSC-NCG mice (5 mice per group). 15 days after inoculation, mice were treated with irradiation, irradiation + Dox, or irradiation + Dox + anti-IL6R antibody. Tumour growth curves were monitored, and tumour volumes and weights were compared at the indicated time points. $n = 3$ independent experiments (**A**–**I**). One of three experiments is shown (**C**). Data are shown as mean ± SD (**A**, **B**, **D**–**I**) or mean ± SEM (**K**, **L**). *P* values were calculated using two-tailed unpaired t test (**D**), one-way ANOVA (**E**–**I**, **L**) or two-way ANOVA (**A**, **B**, **K**). Source data are provided as a Source Data file.

https://doi.org/10.1038/s41467-025-62558-4

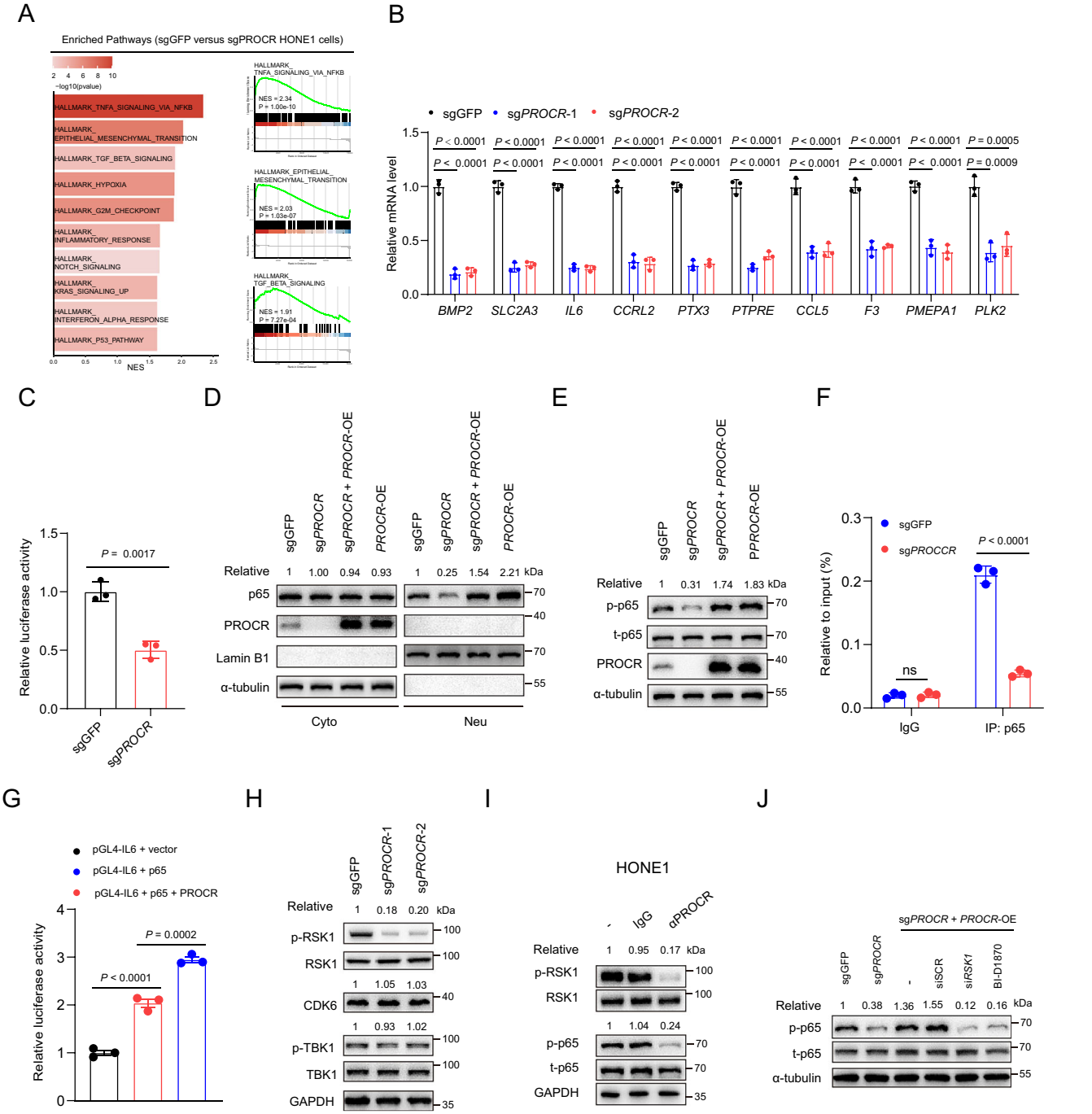

Fig. 4 | PROCR induces p65 activation via RSK1 to promote IL6 transcription. **A** Gene set enrichment analysis (GSEA) showing the top enriched pathways in parental (sgGFP) versus *PROCR*-knockout (sg*PROCR*) HONE1 cells. **B** RT-qPCR results for the mRNA expression of the indicated NF-κB-targeted genes in parental (sgGFP) and *PROCR*-knockout (sg*PROCR*) HONE1 cells. **C** Luciferase assay showing the NF-κB activity in parental (sgGFP) and *PROCR*-knockout (sg*PROCR*) HONE1 cells. **D** Western blot analysis of p65 in cytoplasmic (cyto) and nuclear (neu) fractions of parental (sgGFP), *PROCR*-knockout (sg*PROCR*), and PROCR-rescue (sg*PROCR* + *PROCR*-OE) HONE1 cells. Lamin B1 and α-tubulin were used as nuclear and cytoplasmic markers, respectively. **E** Western blot analysis of total and phosphorylated p65 in parental (sgGFP), *PROCR*-knockout (sg*PROCR*), PROCR-rescue (sg*PROCR* + *PROCR*-OE), and PROCR-OE HONE1 cells. **F** ChIP-PCR detection of the transcriptional regulation of p65 on IL6 in parental (sgGFP) and *PROCR*-knockout (sg*PROCR*) HONE1 cells. **G** Luciferase reporter assays showing the *IL6* promoter activity in p65 or p65 plus PROCR overexpressed HONE1 cells. **H** Western blot analysis of total and phosphorylated RSK1, total and phosphorylated TBK1, and CDK6 in parental (sgGFP) and *PROCR*-knockout (sg*PROCR*) HONE1 cells. **I** Western blot analysis of total and phosphorylated RSK1, total and phosphorylated p65 in HONE1 cells pretreated with IgG or αPROCR. **J** Western blot analysis of total and phosphorylated p65 in parental (sgGFP), *PROCR*-knockout (sg*PROCR*), PROCR-rescue (sg*PROCR* + *PROCR*-OE), PROCR-rescue with *RSK1*-knockdown and PROCR-rescue with BI-D1870 (RSK1 inhibitor) in HONE1 cells. $n = 3$ independent experiments (**B**–**J**). One of three experiments is shown (**D**, **E**, **H**–**J**). Data are shown as mean ± SD (**B**, **C**, **F**, **G**). *P* values were calculated using two-tailed unpaired t test (**C**, **F**) or one-way ANOVA (**B**, **G**). Source data are provided as a Source Data file.

of activated B cells (NF-κB) signalling pathway ranked at the top (Fig. 4A). The NF-κB pathway is highly involved in regulating inflammatory responses, including directly regulating IL-6 expression[28]. More convincingly, through qPCR, we confirmed that the expression of these reported target genes regulated by NF-κB pathway was decreased in *PROCR* knockout HONE1 cells (Fig. 4B). Consistently, by transfecting a luciferase reporter plasmid containing the NF-κB response element sequence into HONE1 cells, we also found that the luciferase signal was reduced after *PROCR* knockout (Fig. 4C). Furthermore, by immunoblotting, we found that p65 nuclear translocation and phosphorylation (S536) were reduced in *PROCR* knockout HONE1 cells and could be rescued by *PROCR* re-expression (Fig. 4D, E). More importantly, when we treated HONE1 cells with the p65 translocation inhibitor JSH-23 or knocked out p65 with CRISPR-CAS9 (Supplementary Fig. 4A), both the mRNA and protein levels of IL-6 were significantly decreased, and the effect of the re-expression of PROCR on the upregulation of IL-6 was abolished under these two conditions (Supplementary Fig. 4B-E). Moreover, using an anti-p65 antibody for chromatin immunoprecipitation (ChIP), we found that the binding of p65 to the IL-6 promoter was reduced after *PROCR* knockout (Fig. 4F). Then, we also constructed a luciferase reporter plasmid driven by the human IL-6 promoter and found that overexpression of PROCR could enhance the transcriptional activity of p65 on IL-6 (Fig. 4G). Consistent with the results obtained from human cells, we found that *PROCR* knockout led to reduced nuclear translocation of p65 in MC38 cells (Supplementary Fig. 4F), and treatment with JSH-23 abolished the PROCR-mediated upregulation of IL-6 in MC38 cells as well (Supplementary Fig. 4G, H).

We then explored the detailed regulatory mechanism on NF-κB pathway by PROCR. Interestingly, it was found that the use of IKK inhibitors (BAY 11-7082 or BMS-345541) only showed faint effects on inhibiting the regulatory effect of PROCR on IL-6 (Supplementary Fig. 4I). More convincingly, *PROCR* knockout did not significantly affect the phosphorylation levels of IKKβ (Supplementary Fig. 4J). Therefore, we screened several other critical kinases (TBK1, RSK1, CDK6) that could directly phosphorylate p65 at S536 and induce nuclear translocation and found that RSK1 activation was weakened after *PROCR* knockout, while the other two kinases showed no significant changes (Fig. 4H). More importantly, we also found that anti-PROCR treatment led to decreased phosphorylation levels of RSK1 and p65 (Fig. 4I, supplementary Fig. 4L). To further clarify the role of RSK1, we used its inhibitor BI-D1870 or transfected targeted siRNA; and found that under RSK1 inhibition, re-expression of PROCR could neither activate p65 nor upregulate IL-6 expression (Fig. 4J, supplementary Fig. 4K).

RSK family members are distinguished by having two kinase domains, N-terminal kinase domain (NTKD) and C-terminal kinase domain (CTKD)[29]. Extracellular signal-regulated kinase (ERK) and PDPK1 were the major molecules activating RSK1. Therefore, we transfected siRNAs targeting *PDPK1* or *ERK1/2* in PROCR-rescue (sg*PROCR* + *PROCR* overexpression) HONE1 cells. It was found that knocking-down of *PDPK1* showed minimal effect, whereas knocking-down of *ERK1/2* almost abolished the enhanced phosphorylation of p65 led by PROCR overexpression (Supplementary Fig. 4M). Consistently, enhancement of S380 phosphorylation of RSK1 and upregulation of IL6 led by overexpression of PROCR was lost after knocking down of *ERK1/2* (Supplementary Fig. 4N, O). More importantly, in doxycycline-dependent, inducible expression of MYC-tagged PROCR HONE1 cells (PROCR-MYC^{TetOn}-PROCR$^{-/-}$(PROCR^{Tet})), we also found that higher levels of PROCR led to stronger phosphorylation of ERK1/2 (Thr202/Tyr204) (Supplementary Fig. 4P). To verify whether PROCR was dependent on ligand activation for its effect on activation RSK1 and consequential IL6 upregulation, we treated HONE1 cells with either activated protein C (aPC), a ligand of PROCR, or purified antibody targeting PROCR and found that aPC enhanced the activation of downstream signalling molecules of PROCR (ERK1/2/RSK1) in a concentration-dependent manner, whereas addition of the antibody showed reversed trend with increasing concentration (Supplementary Fig. 4Q). In contrast, there was no significant effect on RSK1 or ERK activation when PROCR knock-out HONE1 cells were treated with aPC or antibody (Supplementary Fig. 4R-S).

Then, we also explored the mechanism by which PROCR activated ERK1/2. Previous studies identified that PROCR primarily activated two relatively independent downstream signalling pathways which were PROCR-F2R or PROCR-SRC-IGF1R axes[30,31]. Notably, ERK1/2 was found located downstream of the PROCR-SRC-IGF1R axis. Furthermore, we transfected siRNAs targeting *F2R*, *SRC* or *IGF1R* into PROCR-rescue HONE1 cells; consistent with previous studies[31], knocking-down of *SRC* or *IGF1R* nearly abolished the effect of increasing phosphorylation levels of ERK1/2 led by PROCR overexpression; in line with this, there was a concomitant decrease in the phosphorylation levels of RSK1 and p65, while knocking-down of *F2R* did not show any significant effect (Supplementary Fig. 4T). Moreover, knocking-down of *SRC* or *IGF1R* also diminished the upregulation of IL6 induced by PROCR overexpression (Supplementary Fig. 4U). Finally, we also observed that the effects of PROCR on phosphorylation of RSK1 and upregulation of IL6 expression under RT were almost lost after knocking-down of *SRC* or *IGF1R* (Supplementary Fig. 4V-W).

Together, the above data suggested that in a ligand dependent mode, PROCR upregulated IL-6 expression via activation of NF-κB signalling through the SRC-IGF1R-ERK kinase cascade.

Selective autophagic degradation of PROCR via p62 is inhibited under irradiation

We previously found that in multiple cell lines PROCR was upregulated after receiving irradiation. To further confirm the relationship between irradiation and PROCR, we isolated EpCAM-positive cells from fresh NPC tissues. After adhesion, these cells were treated with irradiation, and we found that PROCR was upregulated (Fig. 5A). Then, we detected the levels of PROCR via flow cytometry or qPCR of cells 12 h and 24 h after irradiation and found that the protein levels of PROCR increased significantly at both time points, but the mRNA levels did not change significantly (Fig. 5B, C). Irradiation, as a kind of stress, may lead to translational inhibition[32]. Therefore, we speculated that the upregulation of PROCR expression was due to its irradiation-altered protein stability. We then used cycloheximide (CHX) to determine the degradation half-life of PROCR with and without irradiation; as expected, we found that after irradiation, the degradation half-life of PROCR was prolonged (Fig. 5D). The autophagy-lysosomal pathway and the ubiquitin-proteasome pathway are mainstays for protein degradation in cells[33]. Then, we pretreated cells with MG132 (a proteasome inhibitor) or chloroquine (CQ, a lysosome inhibitor) and exposed these cells to irradiation. We found that after proteasomal inhibition, irradiation still led to upregulation of PROCR; interestingly, inhibiting lysosomes increased baseline levels of PROCR, while no further changes occurred after irradiation (Fig. 5E). Furthermore, when we used Earle's balanced salt solution (EBSS) to induce autophagy, the upregulation of PROCR induced by irradiation was weakened (Fig. 5E). More convincingly, after irradiation, a notable decrease in the colocalization of PROCR-GFP with RFP-LC3B-labelled autophagosomes was observed under confocal microscopy (Fig. 5F). We then analysed changes in autophagic flux after irradiation. However, we found that autophagic flux in HONE1 cells did not change after irradiation (Supplementary Fig. 5A-C). This finding indicated that the upregulation of PROCR was not due to changes in nonselective macroscopic autophagic flow.

Selective autophagy can degrade specific proteins independent of changes in autophagic flux; and autophagic adaptors are the core components. Therefore, we screened currently known selective autophagy receptors (p62, TOLLIP, NDP52, NBR1, TAX1BP1, OPTN,

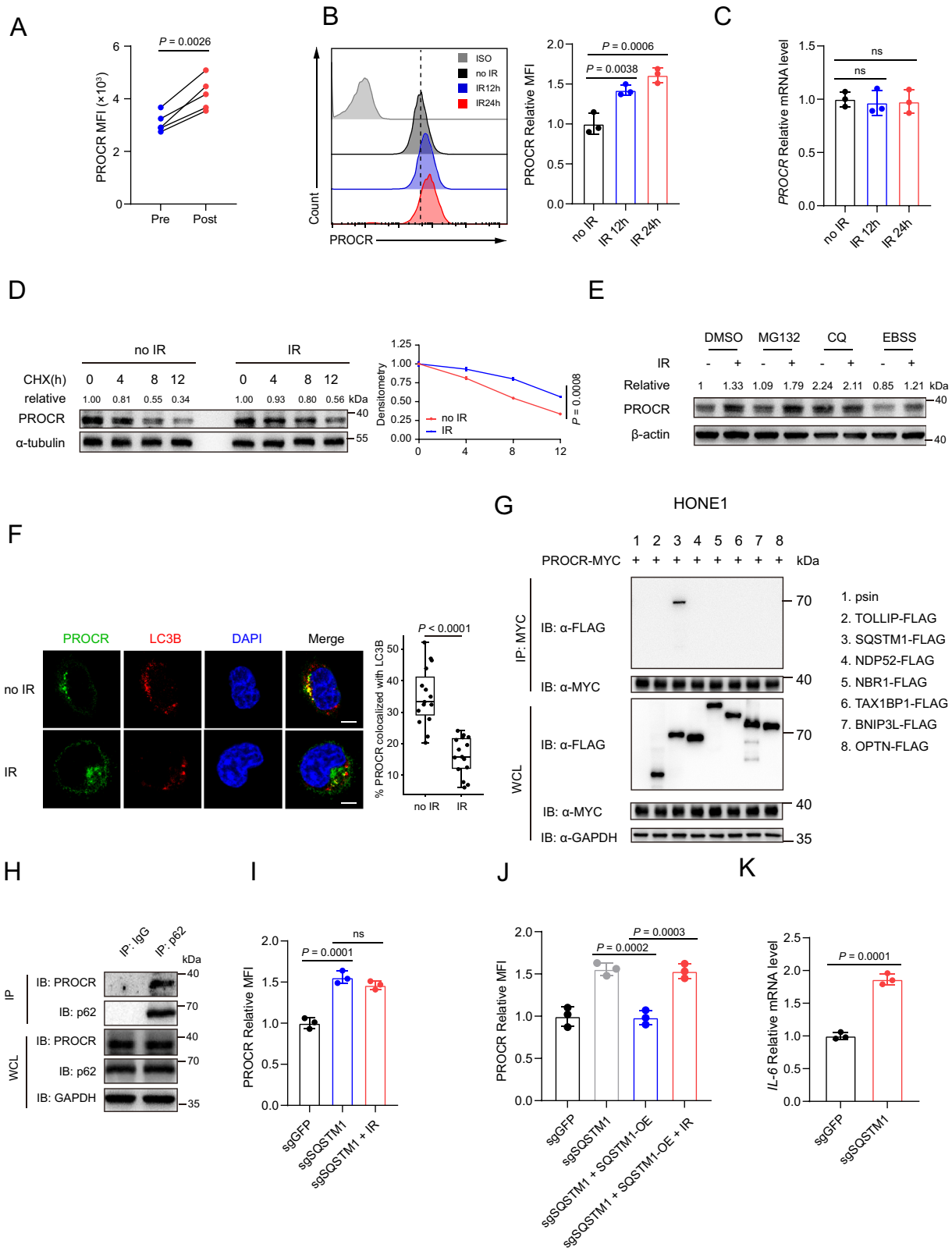

BNIP3L) by coimmunoprecipitation. We found that only p62 could interact with PROCR (Fig. 5G). Furthermore, we confirmed this interaction endogenously (Fig. 5H). To further confirm the role of p62 functionally, we constructed p62 knockout HONE1 cell lines. As expected, we found that after p62 knockout, the protein levels of PROCR were increased compared with those in the cells without knockout; more importantly, in p62 knockout cells, irradiation no longer upregulated PROCR (Fig. 5I, Supplementary Fig. 5D). Consistently, the degradation half-life of PROCR was also prolonged after p62 knockout; under these conditions, irradiation also did not further extend the half-life of PROCR (Supplementary Fig. 5E). When p62 was re-overexpressed, PROCR levels were decreased, and the responsive upregulation to irradiation was restored as well (Fig. 5J). Moreover, *IL6* levels increased in cells with p62 knockout (Fig. 5K). Together, these

Fig. 5 | Selective autophagic degradation of PROCR via p62 is inhibited under irradiation. A Flow cytometry analysis showing PROCR expression of EpCAM$^+$ cells from fresh NPC tissues, treated with or without irradiation ($n = 5$ independent experiments). **B** Flow cytometry analysis showing PROCR expression of HONE1 cells after treatment of radiation for the indicated time intervals. **C** RT-qPCR detection of *PROCR* mRNA expression of HONE1 cells after treatment of radiation for the indicated time intervals. **D** Immunoblots (left) and corresponding greyscale analysis (right) of PROCR in HONE1 cells, treated with CHX for the indicated times, with or without exposure to irradiation. **E** PROCR protein level in HONE1 cells treated with DMSO, MG132, CQ and EBSS, with or without radiation. **F** Immunofluorescence showing localization of PROCR (green) relative to LC3B (red) positive autophagosomes in HONE1 cells, with or without radiation. Graph shows the percentage co-localization ($n = 15$ fields). Scale, 10μm. The boxplots indicate the median (centre), 25th, and 75th percentiles (box boundaries), and minimum and maximum (the whiskers). **G** Coimmunoprecipitation (Co-IP) and immunoblot analysis of HONE1 cells transfected with MYC-tagged PROCR together with FLAG-tagged TOLLIP, SQSTM1, NDP52, NBR1, TAX1BP1, BNIP3L or OPTN. **H** Cell lysates of HONE1 cells were subjected to immunoprecipitation with IgG or anti-p62 antibody. Immunoblot analysis with indicated antibodies were shown. **I** Flow cytometry analysis showing PROCR expression of parental (sgGFP) HONE1 cells, p62-knockout (sg*SQSTM1*) HONE1 cells, and p62-knockout HONE1 cells subjected to radiation treatment (sg*SQSTM1* + IR). **J** Flow cytometry analysis showing PROCR expression of parental (sgGFP) HONE1 cells, p62-knockout (sg*SQSTM1*) cells, p62-rescue (sg*SQSTM1* + *SQSTM1*-OE) cells and p62-rescue cells subjected to radiation treatment (sg*SQSTM1* + *SQSTM1*-OE + IR). **K** RT-qPCR detection of *IL-6* mRNA expression of parental (sgGFP) and p62-knockout (sg*SQSTM1*) HONE1 cells. $n = 3$ independent experiments (**B**–**K**). One of three experiments is shown (**D**, **E**, **G**, **H**). Data are shown as mean ± SD (**B**–**D**, **I**, **J**, **K**). *P* values were calculated using paired t test (**A**), two-tailed unpaired t test (**F**, **K**), one-way ANOVA (**B**, **C**, **I**, **J**), or two-way ANOVA (**D**). Source data are provided as a Source Data file.

findings suggested that irradiation enhanced PROCR expression via suppression of p62-dependent selective autophagy.

The PROCR-p62 interaction is decreased by mTORC1-mediated p62 phosphorylation at S349

We then examined the impact of irradiation on the protein levels of p62 and its interaction with PROCR. The protein levels of p62 did not change after irradiation (Supplementary Fig. 6A), while the interaction between p62 and PROCR was decreased (Fig. 6A). Post-translational modifications, especially phosphorylation, are important in determining the selectivity of p62 for degradation substrates[34,35]. Therefore, by immunoblotting, we analysed the changes in phosphorylation levels of multiple known phosphorylation residuals (T269/S272, S349, S366, S403) that are critical for substrates selection in p62, and found that only the S349 site showed significant changes after irradiation (Fig. 6B). To further identify the key phosphorylation sites, we constructed non-phosphorylatable point mutants of these sites (T269A, S349A, S366A, S403A); by co-transfection with plasmids that overexpressed PROCR, we found that compared with WT p62, both T269A and S403A mutants led to slightly increased levels of PROCR, while S349A induced further decreases in the levels of PROCR, and S366A did not exhibit significant effects on PROCR expression (Fig. 6C). Thus, we speculated that enhanced S349 phosphorylation induced by irradiation led to less binding with PROCR, thereby reducing the degradation of PROCR. As expected, through coimmunoprecipitation, we found that the p62 S349A mutant showed increased binding to PROCR compared with WT p62 (Fig. 6D); more importantly, the p62 S349A mutant increased the entry of PROCR in autolysosomes (Fig. 6E). Consistently, compared with WT p62, p62 S349A further shortened the degradation half-life of PROCR (Fig. 6F) and decreased the levels of *IL6* (Fig. 6G).

Several kinases, including PKCδ, TAK1, CK1, and mTORC1, have been identified to directly phosphorylate p62 at S349 under different conditions[36]. To identify the key kinase involved in our scenario, we pretreated cells with specific kinase inhibitors, including SAR405 (PKCδ), (5Z)−7-oxozeanol (Tak1), CKI7 (CK1) and rapamycin (mTORC1). We found that the upregulation of phosphorylation levels of S349 in p62 induced by irradiation was diminished only when mTORC1 was inhibited (Fig. 6H). To further confirm the role of mTORC1, we used Torin, another mTORC1 inhibitor, or siRNA targeting mTORC1 and obtained similar results to those of rapamycin (Supplementary Fig. 6B). Consistent with this result, we also found that the activity of mTORC1 was increased after irradiation by evaluating the phosphorylation levels of ribosomal protein S6 kinase beta-1 (S6K1), a classic substrate of mTORC1 (Supplementary Fig. 6C). Furthermore, pharmacological inhibition of mTORC1 significantly enhanced the interaction between p62 and PROCR (Fig. 6I), leading to increased colocalization of PROCR and autophagosomes (Supplementary Fig. 6D), a decreased degradation half-life of PROCR (Fig. 6J) and lower levels of PROCR after irradiation (Supplementary Fig. 6E). Consistently, we found that inhibition of mTORC1 decreased PROCR levels in MC38 cells (Supplementary Fig. 6F).

For in vivo experiments, in tumours formed by MC38 wild-type cells, the addition of rapamycin did not further enhance radiotherapy efficacy when anti-PROCR antibody was present; however, in PROCR overexpressing MC38 tumours, PROCR blockade combined with rapamycin exhibited better synergistic effect and further promoted the irradiation-mediated anti-tumour effect (Supplementary Fig. 6G-I, 6J-L). To further substantiate the clinical relevance of our findings, we utilized a humanised mouse model with HONE1$^{\text{PROCR-Tet-On}}$ xenografts. Consistent with our observations in C57BL/6 mice, induced PROCR overexpression dampened the radiation sensitizing effect conferred by rapamycin (Fig. 6K-M). In summary, the above data suggested that inhibiting mTORC1 enhanced the interaction between p62 and PROCR, promoted PROCR autophagic degradation, remodelled antitumour immunity and improved efficacy of radiotherapy.

Higher IL-6 levels indicate a poorer prognosis in NPC

Finally, we explored the clinical relevance and significance of IL-6. By bioinformatic analysis with public datasets, we found that in multiple tumours, especially Liver Hepatocellular Carcinoma (LIHC), Thymoma (THYM), and Kidney Chromophobe (KICH), the expression levels of *PROCR* were strongly positively correlated with *IL6* expression (Supplementary Fig. 7A-C, Supplementary Table 4).

Next, in local cohort of NPC, we conducted IHC staining on 44 NPC tumour samples (the aforementioned tumours in Fig. 1A, B), revealing a positive correlation between IL-6 expression and PROCR expression (Fig. 7A, B). Subsequently, immunohistochemical (IHC) staining was performed on a cohort of 220 paraffin-embedded NPC samples (SYSUCC NPC cohort, Supplementary Table 1), and patients were categorized into a high IL-6 expression group and a low IL-6 expression group for locoregional recurrence rate analysis and Kaplan–Meier analysis. The results demonstrated that patients with high IL-6 expression exhibited a higher probability for locoregional recurrence (Fig. 7C) and significantly shorter disease-free survival (DFS) and overall survival (OS) times (Fig. 7D, E). Furthermore, multivariable Cox regression analysis indicated that IL-6 expression independently served as a prognostic factor for poor OS and DFS in NPC (Supplementary Fig. 7D, E). Collectively, the above findings demonstrated that high IL-6 expression was associated with a compromised antitumour immune response in NPC tumours, as well as a dismal prognosis and an increased risk of relapse in NPC patients.

Discussion

In this study, through multidisciplinary approaches, we identified *PROCR* as an immunosuppressive gene highly related to radiotherapy.

https://doi.org/10.1038/s41467-025-62558-4

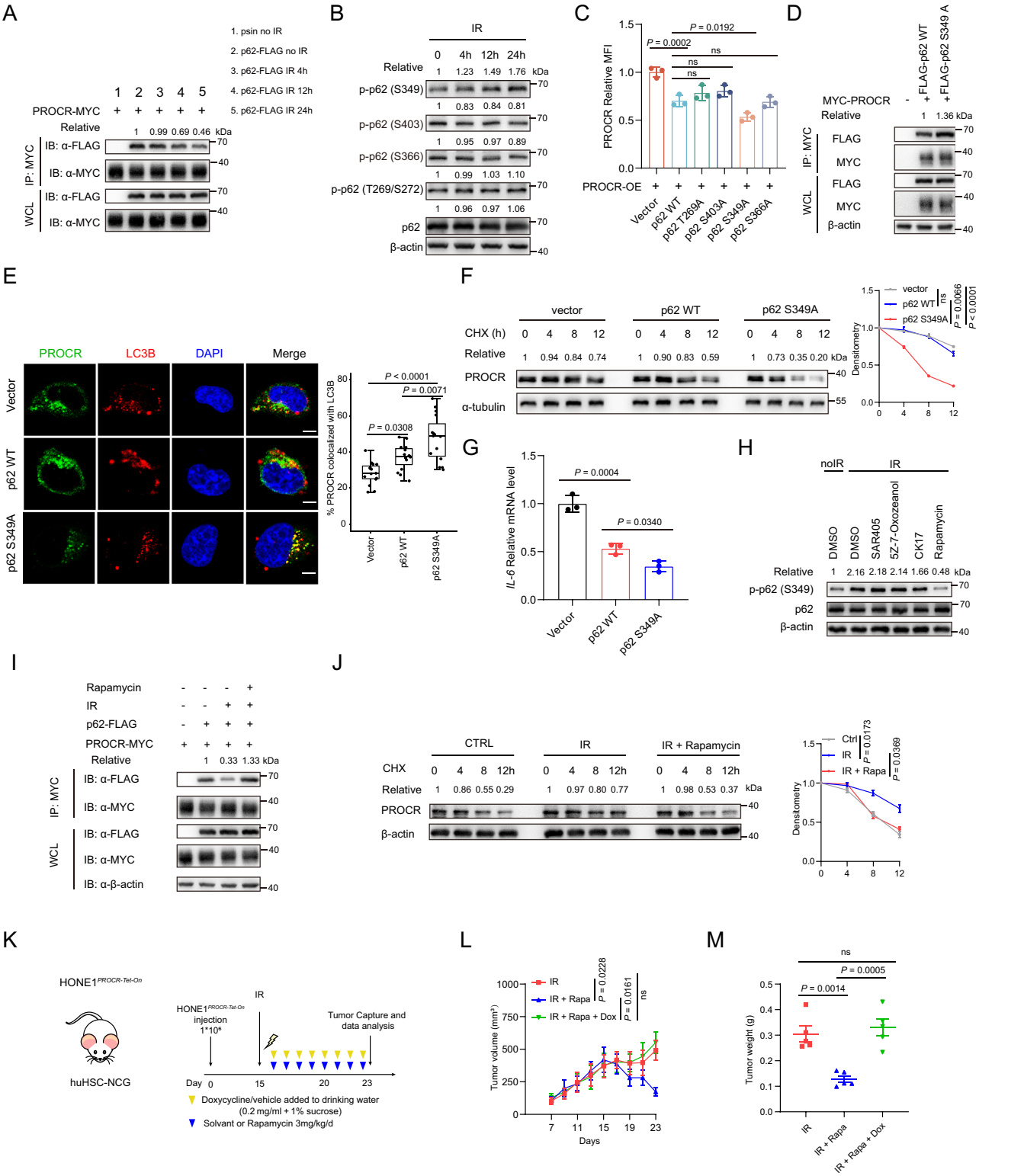

Specifically, first, we determined that by promoting IL-6 secretion, PROCR inhibited Th1 differentiation and impaired $CD8^+$ T-cell function, thus leading to dampened antitumour immunity. Moreover, we found that irradiation could enhance PROCR expression by decreasing its selective autophagy through modulating phosphorylation of p62 via enhancing the kinase activity of mTORC1; indicating that upregulation of PROCR is a kind of inherent feedback of cells to irradiation. Furthermore, in tumours formed on humanized mice of human immune system reconstruction or the C57BL/6 mice of native immune system, targeting PROCR or IL-6 could sensitize radiotherapy through enhancing T-cell dependent antitumour immunity. More importantly, in local NPC cohorts, that the higher expression of PROCR in tumour cells correlated with a lower infiltrated number of Th1 cells and a worse functional state of CD8 + T cells. Meanwhile, higher expression of PROCR or IL-6 was also associated with a poorer response to radiotherapy.

Irradiation-associated antitumour immunity is mainly achieved by inducing immunogenic cell death, increasing tumour-associated

Fig. 6 | PROCR-p62 interaction is diminished by mTOR-mediated p62 phosphorylation at S349. A Coimmunoprecipitation and immunoblot analysis of 293 T cells transfected with MYC-tagged PROCR together with FLAG-tagged p62, with or without radiation treatment, samples were collected at indicated timepoints after radiation. **B** Immunoblots showing phosphorylation of p62 at different sites at indicated timepoints after radiation treatment. **C** Flowcytometry analysis of PROCR in HONE1 cells transfected with PROCR and indicated wild-type p62 or its indicated mutants. **D** Coimmunoprecipitation and immunoblot analysis of 293 T cells transfected with indicated plasmids. **E** Immunofluorescence staining showing co-localization of PROCR and LC3B positive autophagosomes in HONE1 cells transfected with the indicated plasmids ($n = 15$ fields). Scale, 10μm. The boxplots indicate the median (centre), 25th, and 75th percentiles (box boundaries), and minimum and maximum (the whiskers). **F** Immunoblots analysis of PROCR in HONE1 cells transfected with p62-WT or p62-S349A mutant plasmids, treated with CHX for the indicated times. **G** RT-qPCR analysis of *IL6* mRNA level of HONE1 cells transfected with wild-type p62 or its S349A mutant. **H** Immunoblots showing total and S349 phosphorylated p62 of HONE1 cells treated with DMSO, DMSO/SAR405(VPS34 inhibitor)/(5Z)−7-Oxozeanol (Tak1 inhibitor)/CKI7(CK1 inhibitor)/rapamycin (mTORC1 inhibitor) with radiation. **I** Co-immunoprecipitation and immunoblot analysis of 293 T cells transfected with MYC-tagged PROCR and FLAG-tagged p62, treated with radiation, with or without rapamycin (20 nM). **J** Immunoblots analysis of PROCR in HONE1 cells, treated with CHX for the indicated times, treated with radiation, with or without rapamycin (20 nM). **K**–**M** HONE1$^{PROCR\text{-}Tet\text{-}On}$ cells were inoculated into huHSC-NCG mice (1×10^6 HONE1 cells/mouse, 5 mice per group). 15 days after inoculation, mice were treated with irradiation (IR), irradiation + rapamycin (IR + Rapa), or irradiation + rapamycin + doxycycline (IR + Rapa + Dox). Tumour growth curves were monitored, and tumour volumes and weights were compared at the indicated time points. $n = 3$ independent experiments (**A**–**J**). One of three experiments is shown (**A**, **B**, **D**, **F**, **H**, **I**, **J**). Data are shown as mean ± SD (**C**, **F**, **G**, **J**) or mean ± SEM (**L**, **M**). *P* values were calculated using one-way ANOVA (**C**, **E**, **G**, **M**) or two-way ANOVA (**F**, **J**, **L**). Source data are provided as a Source Data file.

antigen exposure, and stimulating the production of cytokines that recruit CD8$^+$ T cells[37]. However, irradiation also exerts immunosuppressive effects by promoting the differentiation of regulatory T cells (Tregs)[38] or myeloid-derived suppressor cells (MDSCs)[39]. Regardless of the mechanism by which the positive and negative effects are generated by irradiation, T-cell-related antitumour immunity is the ultimate convergence point and the factor to adjust the balance towards promotion or inhibition[40,41]. Here, we uncovered an unrecognized role of IL-6 in crosstalk between tumour cells and T cells in the scenario of radiotherapy. Specifically, it was found that irradiation promoted IL-6 secretion by increasing the expression levels of PROCR, leading to inhibited Th1 differentiation and CD8$^+$ T-cell function. Direct blockade of IL-6 or PROCR could tilt the balance of T-cell immunity towards a beneficial antitumour direction. Previous studies identified that IL-6 was mainly induced via recognition of pathogen-associated molecular patterns (PAMPs) and damage-associated molecular patterns (DAMPs) by related pattern recognition receptors (PRRs)[42] expressed on various cell types (macrophages, dendritic cells, lymphocytes, epithelial cells, osteoclasts, hepatocytes, etc.) and mainly mediates acute C-reactive protein induction, increasing serum amyloid[43,44] and vascular permeability[45] or chronic (angiogenesis, fibrosis, etc.) inflammatory responses[44,46]. Tumour cells derived from various tissue types express certain levels of IL-6, which is involved in maintaining the stemness of tumour cells and mediating treatment resistance, metastasis, and tumour recurrence[47–49]. However, in our current study, adding exogenous IL-6 to the culture medium did not reduce the sensitivity of tumour cells to radiotherapy. On the other hand, although IL-6 has been shown to play an important role in inducing Th17 differentiation and inhibiting Treg differentiation and function[50–52], given the complex composition of T-cell subpopulations in the tumour microenvironment, the relationship between IL-6 and antitumour immunity remains unclear. This study further clarified the inhibitory effect of IL-6 on critical antitumour T-cell immunity (Th1/CD8$^+$ T cells). Similarly, in two recent studies, an inhibitory effect on T-cell-dependent antitumour immunity induced by intratumoural IL-6 has also been observed, and blocking IL-6 can enhance the efficacy of immune checkpoint inhibitors[49,53]. From a therapeutic perspective, given that stress induced by various antitumour drugs could inevitably enhance the production of IL-6 and that anti-IL-6 treatment favours the formation of an antitumour immune microenvironment; thus, targeting IL-6 holds promises as an important linkage point that leads to the formation of an effective combination therapy of traditional therapy and immunotherapy.

PROCR was previously identified as a marker of human breast cancer stem cells[18]. Consistent with this finding, we found that in NPC, transformed epithelial cells highly expressing PROCR also showed characteristics of cancer stem cells[19]. Inhibiting programmed cell death process is an important way for cancer stem cells to escape from treatment, especially for radiotherapy. While, in the present study, we found that PROCR showed no significant effect on irradiation-induced cell death. Instead, this group of PROCR-positive cells induced immune evasion in a paracrine manner and ultimately inhibited the efficacy of radiotherapy. However, this phenomenon is not isolated. Although methods and markers for identifying cancer stem cells vary substantially in different systems and tumours from different origins, multiple studies have shown that this subpopulation of cells has a stronger immune evasion ability[54–56]. On the other hand, PROCR was shown to be activated after binding with ligand protein C and transmitting signals downstream[30,31], serving more than just a marker for identification and isolation. Although there was an enhancement of downstream NF-κB/IL6 activation by PROCR in the presence of exogenous protein C addition. In our scenario, we also found that activation of NF-κB/IL-6 by PROCR existed without the addition of protein C. Furthermore, we found that the expression of endogenous protein C was almost undetectable in the cell lines used in this study. Therefore, we speculate that PROCR might have other unknown endogenous ligands continuously activate PROCR. Notably, in local NPC cohorts, through flow cytometry, we found that the higher expression of PROCR in tumour cells correlated with a lower infiltrated number of Th1 cells and a worse functional state of CD8 + T cells; however, by using analytical approaches based on mRNA expression levels in public databases, it was found that the expression of PROCR correlated weakly with Th1 and CD8$^+$ T cells (data not shown).

As an autophagy-selective receptor, p62 can bind cargos through ubiquitin-dependent and ubiquitin-independent modes[57,58]. Post-translational modifications of p62, especially phosphorylation, have important effects on its substrate binding and selection[34]. In the ubiquitin-dependent binding mode, p62 binds to the ubiquitin chain on the substrate mainly through the ubiquitin-binding domain (UBA, 389–434 aa). Phosphorylation of the S403 site within this domain has an important effect on enhancing the binding of p62 to ubiquitin[34]. However, in the case of radiotherapy, the phosphorylation levels of this site did not change significantly. The S349 site is in the KEAP1 interacting region (KIR). From the domain name, we know that p62 directly interacts with KEAP1 through this domain and mediates its autophagic degradation. Phosphorylation of S349 enhances the interaction between p62 and KEAP1. Radiotherapy has a strong ability to induce oxidative stress[12], and according to a previous study, phosphorylation of p62 at S349 is a key anti-oxidative stress response[34], which promotes the degradation of KEAP1, stabilizes NRF2, and induces antioxidant gene expression. Additionally, it has been reported that the activation of mTORC1 is an important mechanism of cellular antioxidant adaptation[59,60]. Here, we found that radiotherapy induced mTORC1-mediated phosphorylation of p62-S349, reducing the binding of p62 to PROCR, which may be due to substrate switching led by enhanced binding to KEAP1 as a byproduct of the intrinsic mechanism

https://doi.org/10.1038/s41467-025-62558-4

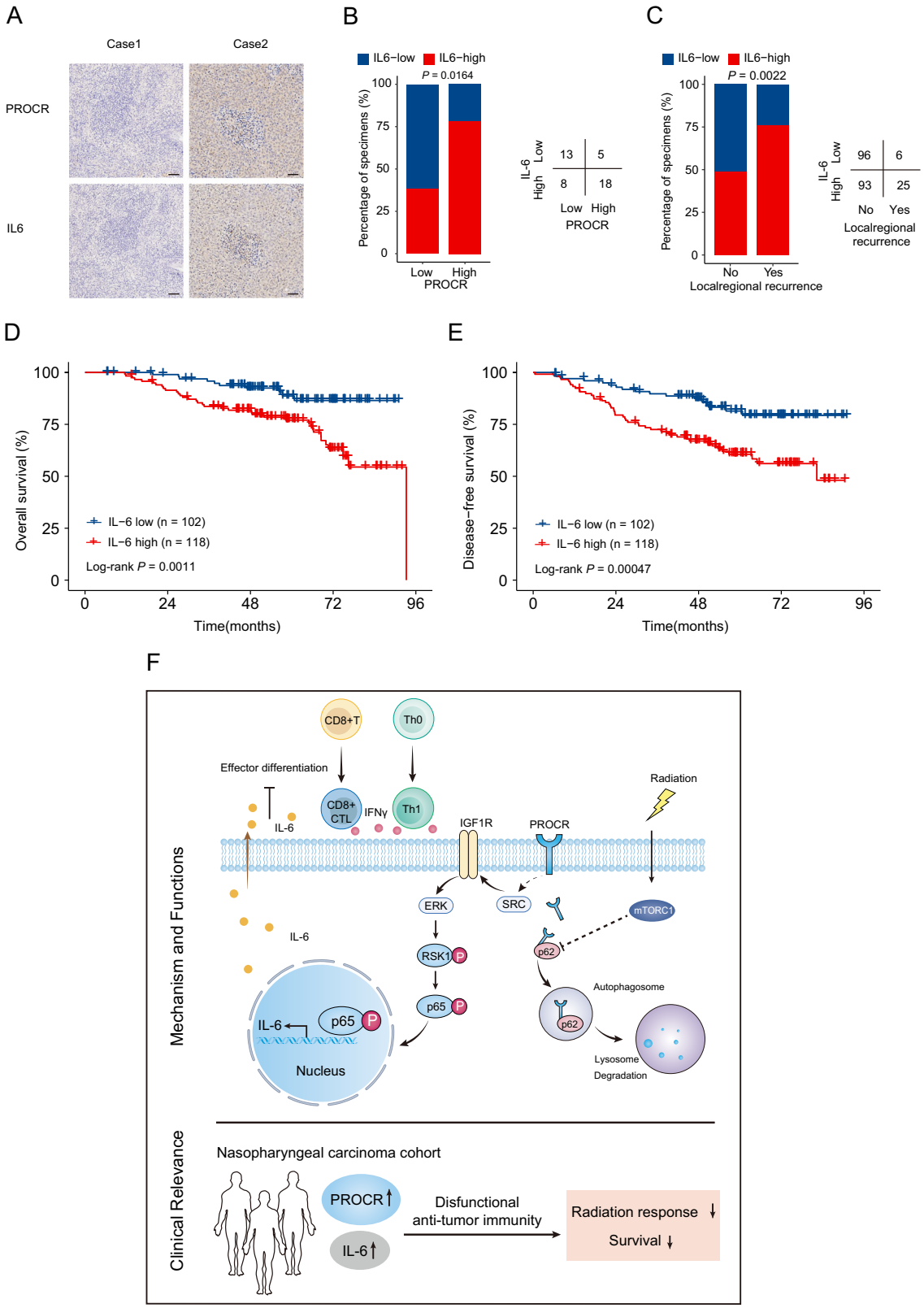

Fig. 7 | Higher levels of IL6 indicates poor prognosis in NPC. A Representative images of IHC staining for PROCR and IL6 expression in NPC tissue samples. Scale bar, 50 μm. **B** Correlation analysis of PROCR expression and IL6 detected by IHC. $n = 44$ independent experiments. The P value was determined using the two-tailed χ^2 test. **C** Correlation analysis of IL6 expression and locoregional recurrence status after radical chemoradiotherapy. $n = 220$ independent experiments. The P value was determined using the two-tailed χ^2 test. Kaplan–Meier analysis of overall survival (**D**) and disease-free survival (**E**) based on the IL6 expression level. The analysis includes 102 patients in the IL-6 low group and 118 patients in the IL-6 high group. The P values were determined using the log-rank test. **F** Proposed working model of PROCR. Mechanistically, PROCR engages Src kinase to transactivate IGF-1R, leading to the activation of ERK and RSK1, which enhances IL-6 secretion through NFκB pathway and inhibits Th1 and $CD8^+$CTL differentiation. PROCR is degraded by p62-mediated selective autophagy, which is inhibited by radiation. Source data are provided as a Source Data file.

to prevent overpowering ROS. More importantly, in addition to increasing cytotoxic sensitivity, interfering with mTORC1 can influence the direction of immune microenvironment reprogramming to more potent antitumour immunity. In summary, we believe that the immune reprogramming induced by radiotherapy depends on the synergistic effect of targets activated by oxidative stress-related small molecules.

Methods

Ethics statement

This study was approved by the Institutional Ethical Review Boards of Sun Yat-sen University Cancer Centre (SYSUCC, Guangzhou, China) (B2022-799). Fully informed consent was obtained from all patients and was in compliance with the Declaration of Helsinki (version 2013). All patients with nasopharygeal carcinoma received radical radiotherapy as an integral component of the standard treatment protocol. Animal experiments in this study were approved by the Experimental Animal Ethics Committee, Sun Yat-sen University (2022002191). All animal experiments were performed in the Animal Experiment Centre of Sun Yat-sen University. Tumour volume was calculated using the following formula: 0.5 × length × width^2. The maximum tumour volume allowed by ethics committee was 2000mm^3 and was not exceeded in our experiments.

Human tissue specimens

All NPC tissue samples from SYSUCC were obtained before treatment, including fresh tissues and paraffin-embedded NPC tissue sections. All patients with nasopharygeal carcinoma received radical radiotherapy as an integral component of the standard treatment protocol. The clinical characteristics of the cohort used for survival analysis are listed in Supplementary Table 1.

IHC analysis

Paraffin-embedded NPC tissue sections were subjected to deparaffinization, rehydration, inactivation of endogenous peroxidase, antigen retrieval, blocking with immunostaining blocking buffer, and incubation with primary antibodies at 4 °C overnight. The next day, tissue sections were incubated with HRP-conjugated rabbit/mouse secondary antibodies (Dako) according to the manufacturer's instructions. Images were obtained with an AxioVision Rel.4.6 computerized image analysis system (Carl Zeiss). All sections were scored by two experienced pathologists according to the immunoreactive score (IRS) system. The staining intensity score was defined as follows: 0, negative staining; 1, weak staining; 2, moderate staining; and 3, strong staining. The positive rate score was defined as follows: 1, <10%; 2, 10–35%; 3, 35–70%; 4, >70%. The total score of indicated proteins was calculated as the product of the intensity score and the positive rate score. Sections with an IRS score of 0-6 were categorized as low, while those with a score of 7–12 were categorized as high. The antibodies used are listed in Supplementary Table 3. The double IHC (dIHC) staining was conducted according to the manufacturer's protocol (ZSGB-BIO, #DS-0003).

Cell culture and treatment

The human NPC cell lines HONE1 and SUNE1 were provided by Professor Mu-Sheng Zeng at Sun Yat-sen University Cancer Centre (Guangzhou). The MC38 murine colon adenocarcinoma cells and HEK293T cells were provided by Professor Bo Huang at Chinese Academy of Medical Sciences (CAMS) & Peking Union Medical College (Beijing). Human tumour cell lines A375 (melanoma) and HCT116 (colorectal tumour) were obtained from the China Centre for Type Culture Collection. HONE1, SUNE1, A375, HCT116 and MC38 were cultured in RPMI-1640 medium, and HEK293T were cultured in DMEM (Invitrogen), supplemented with 10% fetal bovine serum (FBS; Gibco). All the cells were cultured for less than 2 months, and tested for mycoplasma contamination. A375 and HCT116 were authenticated by the supplier using STR fingerprint analysis prior to delivery, other cell lines mentioned were not authenticated.

Cells were seeded in a culture plate one day prior to treatment with radiation or an inhibitor after complete adherence. Cells were treated with a single fraction of 4 Gy, unless otherwise indicated, using the RS-2000-PRO-225 Biological Irradiator (1.827 Gy/min).

Anti-mouse IL-6R monoclonal antibody (2 mg/ml, BioXCell) was used to block IL-6 signalling. Torin1 (1 mM, Macklin) was used to inhibit mTOR and activate autophagy. Activated Protein C (#P2200-.1MG, Sigma-Aldrich) was used to stimulate PROCR signalling. Anti-human PROCR purified antibody (#351902, BioLegend) and anti-mouse PROCR antibody (#16-2012-83, eBioscience) was used to block PROCR signalling.

CRISPR/Cas9 genome editing

To generate indicated knock-out cells, optimal sgRNA target sequences (Supplementary Table 2) were designed using Benchling. The annealed guide RNA oligonucleotides were inserted into a PX458 vector (Addgene) digested with the BbsI restriction enzyme. Cells were seeded at 60% confluence, followed by transfection of sgRNAs (1 μg). Cells were sorted for GFP-positive cells. The cells were diluted for single cells and seeded into 96-well plates. The knock-out efficiency was validated by flow cytometry.

Plasmid construction and transfection

The coding sequence of indicated genes were amplified with PCR and cloned into the pSin-EF2-puro and to construct the following plasmids: pSin-EF2-puro-PROCR, pSin-EF2-puro-PROCR-MYC, pSin-EF2-puro-SQSTM1, pSin-EF2-puro-SQSTM1-T269A, pSin-EF2-puro-SQSTM1-S403A, pSin-EF2-puro-SQSTM1-S349A, pSin-EF2-puro-SQSTM1-S366A, pSin-EF2-puro-SQSTM1-mCherry, pSin-EF2-puro-LC3B-mCherry. Plasmids with human full-length p62, NDP52, NBR1, TAX1BP1, Tollip, Optn and BNIP3L cDNA (with fused C-terminal FLAG tag) subcloned into pcDNA3.1 vector (Invitrogen) were a gift from Professor Zhu Xiaofeng (Sun Yat-sen University).

Cell transfection and lentiviral infection

HEK293T cells were co-transfected with pSin-EF2-puro based constructed vector, pSPAX2, and pMD2.G. Eight hours after transfection, the culture medium was changed to Lonza Ultra-culture medium. After 48 hours, the cell virus supernatant was collected, concentrated and used to infect indicated tumour cell lines. Stable cell lines were infected with lentiviral particles produced by HEK-293T cells and selected using puromycin (1 μg/ml). qRT-PCR, flow cytometry, and western blot were used to confirm the transduction efficiency.

Quantitative real-time PCR (qRT-PCR)

RNA was extracted from indicated cells, and reverse transcription of the first-strand cDNA was performed using a reverse-transcription kit (Promega). The qRT-PCR assay was conducted on the Bio-Rad SPX (96 or 384) system with a 2X SYBR Green mix (Life, Carlsbad, CA, USA). The data were normalized to the expression of GAPDH. The sequences of the primers are listed in Supplementary Table 2.

Western blot analysis

Protein was extracted from the cells using IP buffer (Beyotime) containing protease and phosphatase inhibitors (Beyotime), separated by SDS–polyacrylamide gels, and then transferred to NC membranes (Merck Millipore). The membranes were blocked at room temperature and then incubated overnight at 4 °C with primary antibodies. According to the manufacturer's recommended dilution, primary antibodies against β-actin, α-tublin, anti-gamma H2A.X, GAPDH, STAT1, phospho-STAT1, IRF3, phospho-IRF3, p65, phospho-p65, Lamin B1, RSK1, phospho-RSK1, CDK6, TBK1, phospho-TBK1, IKKβ, phosphor-IKKβ, LC3, PROCR, p62, phospho-p62(S349), phospho-p62(S403),

phospho-p62(S366), phospho-p62(Th269/Ser272), anti-FLAG, anti-MYC, phospho-p70 S6K were used. Peroxidase conjugated secondary antibody (CST) was used, and the antigen-antibody reaction was visualized by enhanced chemiluminescence assay (ECL, Thermo). The antibodies used are listed in Supplementary Table 3.

Short interfering RNAs transfer

SiRNA targeting ERK1/2 was purchased from Cell Signalling Technology (# 6560S), other short interfering RNAs (siRNAs) targeting indicated genes were designed and synthesized by GenePharma (Shanghai, China). Lipo3000 was used to transfect according to the manufacturer's instructions, and knock-down efficiency was validated by qPCR or western blot. The sequences of the primers are listed in Supplementary Table 2.

Subcellular fractionation

Nuclear and cytosolic fractions were isolated from the cells using a nuclear/cytosolic fractionation kit (Thermo Scientific™) according to the manufacturer's protocol.

ELISA

Cells were cultured in 1640 with 10% FBS under indicated conditions. The supernatant was harvested and used for subsequent IL-6 and IL8 (Neobioscience). All experiments were performed according to the manufacturer's instructions.

Cytokine profiling

The secretion of multiple cytokines were measured simultaneously by a multiplex bead array using the Cytokine & Chemokine 34-Plex Human ProcartaPlex™ Panel (Invitrogen, EPX340-12167-901) according to the manufacturer's protocol.

Cell proliferation

The CCK-8 assay was used to detect cell proliferation. Cells (1×10^3) were seeded in 96-well plates, incubated for 0–5 days, and stained using CCK-8 (Dojindo, Tokyo, Japan). The absorbance was determined at 450 nm using a spectrophotometer. A total of 120 h later, cell viability was evaluated using the CCK-8 assay.

Flow cytometry

For the NPC biopsy tissues or murine tumour samples, the tissues were digested into a single cell solution using collagenase IV (17104019, Invitrogen). For cell surface marker analysis, cells were resuspended in PBS and stained with fluorescent-conjugated antibodies against PROCR, CD45, CD4, CD8 for 30 min at 4 °C. For IFNγ, Intracellular Fixation & Permeabilization Buffer Set (Invitrogen) was used according to the manufacturer's instructions. The antibodies used are listed in Supplementary Table 3. For apoptosis analysis, cells exposed to radiation with indicated dosage were dissociated by 0.25% trypsin (EDTA free), washed with PBS and collected by centrifugation, and then stained with annexin V/7-AAD Apoptosis Detection Kit (Cat# 577 640930, BioLegend) following the manufacturer's instructions. The stained cells were detected with a cytoFLEX flow cytometer, and the data were analysed using the FlowJo software.

In vitro Th1 differentiation

Naive T cells from young mice were stimulated with plate-bound anti-CD3 and anti-CD28 Abs (both eBioscience) in the presence of IL-12 (8 ng/ml; Wako) and anti-IL-4 Ab (10 μg/ml) for Th1 differentiation. Tumour-infiltrating immune cells were isolated via fluorescence-activated cell sorting (FACS) using a Beckman Coulter Moflo flow cytometer. Standard criteria, based on forward scatter width (FSC-W) versus area (FSC-A), were applied to exclude doublets and capture singlets. $CD4^+$ T cells and $CD8^+$ T cells were sorted using gates defined by $CD45^+CD4^+$ and $CD45^+$ $CD8^+$, respectively (Supplementary Fig. 2A).

Construction of human HER2-CAR T cells

The scFv fragment of HER2 from monoclonal antibody 4D5 linked the CD8α-chain hinge and transmembrane region with CD3ζ and CD28 intracellular signalling domains, and this cassette was inserted into the lentiviral vector provided by the Obioo Bioscience Company[61]. The transduction procedure was initiated by stimulating $CD8^+$ T cells with CD3/CD28 activator beads (Invitrogen) according to the instruction provided by the manufacturer with recombinant human IL-2 at a final concentration of 100 U/ml in X-VIVO 15 culture medium (Lonza) containing 5% FBS. Cells were harvested for lentiviral transduction on day 2 and resuspended in the same medium. The supernatants containing lentiviruses were added to the medium at the multiplicity of infection of 1:10, and the plates were coated with RetroNectin [CH-296; Takara Bio, Otsu, Japan; coated using CH-296 (10 mg/ml)] according to the manufacturer. Then, cells were centrifuged at 1000 g for 2 hours at 32 °C and incubated at 37 °C for 6 hours. The infection rates were quantified with flow cytometry after 2 days. The transfection efficiency was evaluated by flow cytometry on days 3 and 5 after lentivirus transduction and at the end of culture. The transfection efficiency was around 40%. For in vitro experiments, we cultured CAR T cells for 5 to 7 days. These T cells grew logarithmically during the period of expansion.

Dual-luciferase reporter assay

The pGMR-TK Renilla and NF-κB luciferase reporter plasmids were purchased from Genomeditech. Parental (sgGFP) or PROCR-knockout (sgPROCR) HONE1 cells were transfected with pGMR-TK Renilla, a NF-κB luciferase reporter plasmid after seeding in 24-well plates for 12 h. After transfection for 36–48 h, the Dual Luciferase Assay Kit (Promega) was used to analyse the relative luciferase activity following the manufacturer's protocol, which was measured with a GloMax 96 Microplate Luminometer (Promega).

Promoter of IL6 was cloned into pGL4.10[*luc2*] vector (Promega). Cells were seeded into 12-well plates and co-transfected with plasmids encoding p65, PROCR, or empty vector, along with IL6 promoter-reporter plasmid and Renilla luciferase plasmid for 12 h. After transfection for 24 h, the Dual Luciferase Assay Kit (Promega) was used to detect the luciferase activity, and the data were normalized to Renilla luciferase activity.

Chromatin Immunoprecipitation (ChIP) Assay

The ChIP assay was carried out using A Pierce Magnetic ChIP Kit (Cat# 26157, Thermo Fisher Scientific). In brief, cells were cross-linked and chromatin was sonicated to obtain 200- to 500-bp DNA fragments. The samples were immunoprecipitated with anti-NFκB antibodies (8242S, CST) or anti IgG (2729S, CST) antibodies. The purified DNA was used for qRT-PCR, and the sequence of the primer is as follows: IL6 forward: 5'- AGGACTGGAGATGTCTGAGGCTCATTCT −3'.

Co-immunoprecipitation (co-IP) assay

The extracted proteins were immunoprecipitated with magnetic beads covalently coupled with nano tag-antibodies (Pierce). The volume of beads required and the incubation time were in accordance with the relevant manufacturer's instructions. In endogenous co-IP assay, protein immunoprecipitation was performed at 4 °C overnight with antibodies at the recommended dilution. Pierce™ Protein A/G Magnetic Beads (Thermo Scientific) were then used to capture the immune complexes at room temperature for 1 h, which were washed with IP wash buffer and then subjected to immunoblotting analysis.

Immunofluorescence and confocal microscopy

For immunofluorescent staining of p65, the cells were fixed with 4% paraformaldehyde for 15 min at room temperature, washed with PBS, and permeabilized with 0.1% Triton X-100 in PBS for 15 min. After permeabilization, cells were blocked and incubated with rabbit-anti-

human NFκB primary antibody (8242S, CST, 1:400). Incubation of secondary antibodies (Alexa Fluor 488, Invitrogen) were carried out for 1 h at room temperature. DAPI was then used to stain the nuclei. Fluorescence images were captured using a confocal laser-scanning microscope (LSM880, Zeiss).

Tumour growth, treatment and analyses

Six-week-old female, specific pathogen-free/SPF, BALB/c nude mice and C57BL/6 mice were purchased from Charles River Laboratories (Zhejiang). Mice were subcutaneously inoculated with 1×10^6 MC38 cells. The humanised mice (huHSC-NCG) were purchased from GemPharmatech, which is established by transplanting human hematopoietic stem cells ($CD34^+$HSC) into irradiated NCG mice, leading to the differentiation and production of various hematopoietic or immune cells such as T cells, B cells, and NK cells, thereby obtaining a humanized model of the immune system. HONE1 cells were used to establish NPC xenograft in huHSC-NCG following the aforementioned schedule. After random grouping of mice, the mice were anaesthetized with isoflurane and fixed, the mice body were covered with lead plates (>5 mm), and then the tumours were locally irradiated with a single fraction (4 Gy) using an RS-200-PRO-225 Biological Irradiator (1.827 Gy/min) when tumours reach approximately 200 mm^3. PROCR neutralizing antibody (200 μg per mouse, Thermo Fisher Scientific) were administered intraperitoneally for PROCR blockade in experiments using C57BL/6. Anti-human PROCR antibody (200 μg per mouse, Biolegend) were administered intraperitoneally for PROCR blockade in experiments using huHSC-NCG. Anti-human CD4 (100 μg per mouse, twice weekly, clone: RPA-T4, Cat # 300570) and CD8 (100μg per mouse, twice weekly, clone SK1, Cat # 344702) were administered intraperitoneally for depletion of CD4 and CD8 T cells, respectively, in humanized mouse models. Anti-CD3ε antibody (200μg per mouse, every third day, BioXCell) were administered intraperitoneally for depletion of overall T cell. Anti-CD4 antibody (100μg per mouse, BioXCell) were administered intraperitoneally for CD4 depletion, from day 3 post tumour inoculation, twice weekly. Anti-CD8 antibody (100 μg per mouse, BioXCell) were administered intraperitoneally for CD8 depletion, every 6 days from day3 post tumour inoculation. Recombinant mouse IL-6 protein (R&D systems, 406-ML) 200 ng/50 μL/body or 50 μL of PBS was directly injected into the tumours every 4 days. Anti-IL6R monoclonal antibody (200 μg per mouse, BioXCell) were administered intraperitoneally for IL-6 signal blockade. The tumours were monitored every other day. The tumour tissues were digested into single-cell suspensions, and infiltrating immune cells were analysed by flow cytometry. To evaluate the proportion of $IFNγ^+$ $CD4^+$ and $CD8^+$ T cells, single-cell suspensions from MC38 tumours were treated with Cell Stimulation Cocktail (plus protein transport inhibitors) (00-4975-93, Thermo Scientific) for 4 h before staining, and the percentages of $CD45^+CD4^+IFNγ^+$ or $CD45^+CD8^+IFNγ^+$ T cells were determined.

Bioinformatics analysis

GSEA was conducted with the R package clusterProfiler (version 3.12.0) based on gene expression matrices.

Statistical analysis and reproducibility

Data are presented as the mean ± SD or mean ± SEM of at least three independent experiments. Statistical analysis was performed using GraphPad Prism 9.0 software or SPSS 25 (IBM). Two-tailed unpaired Student's t-test were used to compare between two group (treatments vs. control). One-way ANOVA or two-way ANOVA models were performed for more than two groups to calculate *P* values. Survival analysis was estimated by Kaplan–Meier methods. A multivariable Cox proportional hazards model was used to estimate independent prognostic factors. The statistical details including the statistical tests used, exact value of n, and precision measures (mean ± SD or SEM) were all specified in the figure legends unless otherwise indicated. A *P* value of <0.05 was considered statistically significant.

Reporting summary

Further information on research design is available in the Nature Portfolio Reporting Summary linked to this article.

Data availability

The raw sequence data of RNA-seq data generated in this study have been deposited in the GEO database under the accession code GSE282897. TCGA datasets were obtained from TIMER2.0 [http://timer.cistrome.org/]. All the other data supporting the findings of this study are included in the article and its Supplementary Information files. The key raw data have been deposited to Research Data Deposit public platform [https://www.researchdata.org.cn], with the approval RDD number as RDDB2024552913. All key raw data deposited are also included in the source data file provided with this paper. Source data are provided with this paper.

References

1. Harrington, K. J. et al. Guidelines for preclinical and early phase clinical assessment of novel radiosensitisers. *Br. J. Cancer* **105**, 628–639 (2011).
2. Goldstein, M. & Kastan, M. B. The DNA damage response: implications for tumor responses to radiation and chemotherapy. *Annu Rev. Med.* **66**, 129–143 (2015).
3. Weichselbaum, R. R., Liang, H., Deng, L. & Fu, Y. X. Radiotherapy and immunotherapy: a beneficial liaison?. *Nat. Rev. Clin. Oncol.* **14**, 365–379 (2017).
4. Herrera, F. G., Bourhis, J. & Coukos, G. Radiotherapy combination opportunities leveraging immunity for the next oncology practice. *CA Cancer J. Clin.* **67**, 65–85 (2017).
5. Harding, S. M. et al. Mitotic progression following DNA damage enables pattern recognition within micronuclei. *Nature* **548**, 466–470 (2017).
6. Mackenzie, K. J. et al. cGAS surveillance of micronuclei links genome instability to innate immunity. *Nature* **548**, 461–465 (2017).
7. Deng, L. et al. STING-dependent cytosolic DNA sensing promotes radiation-induced type I interferon-dependent antitumor immunity in immunogenic tumors. *Immunity* **41**, 843–852 (2014).
8. Guan, J. et al. MLH1 deficiency-triggered DNA hyperexcision by exonuclease 1 activates the cGAS-STING pathway. *Cancer Cell* **39**, https://doi.org/10.1016/j.ccell.2020.11.004 (2021).
9. Li, J. Y. et al. TRIM21 inhibits irradiation-induced mitochondrial DNA release and impairs antitumour immunity in nasopharyngeal carcinoma tumour models. *Nat. Commun.* **14**, 865 (2023).
10. Domingo, E. et al. Identification and validation of a machine learning model of complete response to radiation in rectal cancer reveals immune infiltrate and TGFβ as key predictors. *EBioMedicine* **106**, 105228 (2024).
11. Zhang, Y. et al. CD39 inhibition and VISTA blockade may overcome radiotherapy resistance by targeting exhausted CD8+ T cells and immunosuppressive myeloid cells. *Cell Rep. Med.* **4**, 101151 (2023).
12. Baumann, M. et al. Radiation oncology in the era of precision medicine. *Nat. Rev. Cancer* **16**, 234–249 (2016).
13. Salmon, T. B., Evert, B. A., Song, B. & Doetsch, P. W. Biological consequences of oxidative stress-induced DNA damage in Saccharomyces cerevisiae. *Nucleic Acids Res.* **32**, 3712–3723 (2004).
14. Hwang, I. et al. Cellular stress signaling activates type-I IFN response through FOXO3-regulated lamin posttranslational modification. *Nat. Commun.* **12**, 640 (2021).
15. Gorrini, C., Harris, I. S. & Mak, T. W. Modulation of oxidative stress as an anticancer strategy. *Nat. Rev. Drug Discov.* **12**, 931–947 (2013).

16. Blanpain, C., Mohrin, M., Sotiropoulou, P. A. & Passegue, E. DNA-damage response in tissue-specific and cancer stem cells. *Cell Stem Cell* **8**, 16–29 (2011).
17. Kobayashi, C. I. & Suda, T. Regulation of reactive oxygen species in stem cells and cancer stem cells. *J. Cell. Physiol.* **227**, 421–430 (2012).
18. Wang, D. et al. Protein C receptor is a therapeutic stem cell target in a distinct group of breast cancers. *Cell Res.* **29**, 832–845 (2019).
19. Zhang, P. et al. Protein C receptor maintains cancer stem cell properties via activating lipid synthesis in nasopharyngeal carcinoma. *Signal Transduct. Target Ther.* **7**, 46 (2022).
20. Jiang, N. et al. Fatty acid oxidation fuels glioblastoma radioresistance with CD47-mediated immune evasion. *Nat. Commun.* **13**, 1511 (2022).
21. Hoy, A. J., Nagarajan, S. R. & Butler, L. M. Tumour fatty acid metabolism in the context of therapy resistance and obesity. *Nat. Rev. Cancer* **21**, 753–766 (2021).
22. Snaebjornsson, M. T., Janaki-Raman, S. & Schulze, A. Greasing the wheels of the cancer machine: the role of lipid metabolism in cancer. *Cell Metab.* **31**, 62–76 (2020).
23. Barker, H. E., Paget, J. T., Khan, A. A. & Harrington, K. J. The tumour microenvironment after radiotherapy: mechanisms of resistance and recurrence. *Nat. Rev. Cancer* **15**, 409–425 (2015).
24. McLaughlin, M. et al. Inflammatory microenvironment remodelling by tumour cells after radiotherapy. *Nat. Rev. Cancer* **20**, 203–217 (2020).
25. Hung, M. H. et al. Tumor methionine metabolism drives T-cell exhaustion in hepatocellular carcinoma. *Nat. Commun.* **12**, 1455 (2021).
26. Taifour, T. et al. The tumor-derived cytokine Chi3l1 induces neutrophil extracellular traps that promote T cell exclusion in triple-negative breast cancer. *Immunity* **56**, 2755–2772.e2758 (2023).
27. Pylayeva-Gupta, Y., Lee, K. E., Hajdu, C. H., Miller, G. & Bar-Sagi, D. Oncogenic Kras-induced GM-CSF production promotes the development of pancreatic neoplasia. *Cancer Cell* **21**, 836–847 (2012).
28. Brasier, A. R. The nuclear factor-kappaB-interleukin-6 signalling pathway mediating vascular inflammation. *Cardiovasc. Res.* **86**, 211–218 (2010).
29. Anjum, R. & Blenis, J. The RSK family of kinases: emerging roles in cellular signalling. *Nat. Rev. Mol. Cell Biol.* **9**, 747–758 (2008).
30. Liu, C. et al. Procr functions as a signaling receptor and is essential for the maintenance and self-renewal of mammary stem cells. *Cell Rep.* **38**, 110548 (2022).
31. Wang, D. et al. Protein C receptor stimulates multiple signaling pathways in breast cancer cells. *J. Biol. Chem.* **293**, 1413–1424 (2018).
32. Bresson, S. et al. Stress-induced translation inhibition through rapid displacement of scanning initiation factors. *Mol. Cell* **80**, 470–484.e478 (2020).
33. Ding, W. X. & Yin, X. M. Sorting, recognition and activation of the misfolded protein degradation pathways through macroautophagy and the proteasome. *Autophagy* **4**, 141–150 (2008).
34. Matsumoto, G., Wada, K., Okuno, M., Kurosawa, M. & Nukina, N. Serine 403 phosphorylation of p62/SQSTM1 regulates selective autophagic clearance of ubiquitinated proteins. *Mol. Cell* **44**, 279–289 (2011).
35. Ichimura, Y. et al. Phosphorylation of p62 activates the Keap1-Nrf2 pathway during selective autophagy. *Mol. Cell* **51**, 618–631 (2013).
36. Sánchez-Martín, P. & Komatsu, M. p62/SQSTM1—steering the cell through health and disease. *J. Cell Sci.* **131**, https://doi.org/10.1242/jcs.222836 (2018).
37. Rodriguez-Ruiz, M. E., Vitale, I., Harrington, K. J., Melero, I. & Galluzzi, L. Immunological impact of cell death signaling driven by radiation on the tumor microenvironment. *Nat. Immunol.* **21**, 120–134 (2020).
38. Ji, D. et al. Combination of radiotherapy and suppression of Tregs enhances abscopal antitumor effect and inhibits metastasis in rectal cancer. *J Immunother. Cancer* **8**, https://doi.org/10.1136/jitc-2020-000826 (2020).
39. Xu, J. et al. CSF1R signaling blockade stanches tumor-infiltrating myeloid cells and improves the efficacy of radiotherapy in prostate cancer. *Cancer Res.* **73**, 2782–2794 (2013).
40. Chen, D. S. & Mellman, I. Oncology meets immunology: the cancer-immunity cycle. *Immunity* **39**, 1–10 (2013).
41. Giles, J. R., Globig, A. M., Kaech, S. M. & Wherry, E. J. CD8(+) T cells in the cancer-immunity cycle. *Immunity* **56**, 2231–2253 (2023).
42. Takeuchi, O. & Akira, S. Pattern recognition receptors and inflammation. *Cell* **140**, 805–820 (2010).
43. Del Giudice, M. & Gangestad, S. W. Rethinking IL-6 and CRP: why they are more than inflammatory biomarkers, and why it matters. *Brain Behav. Immun.* **70**, 61–75 (2018).
44. Gabay, C. & Kushner, I. Acute-phase proteins and other systemic responses to inflammation. *N. Engl. J. Med.* **340**, 448–454 (1999).
45. Maruo, N., Morita, I., Shirao, M. & Murota, S. IL-6 increases endothelial permeability in vitro. *Endocrinology* **131**, 710–714 (1992).
46. Kopf, M. et al. Impaired immune and acute-phase responses in interleukin-6-deficient mice. *Nature* **368**, 339–342 (1994).
47. Johnson, D. E., O'Keefe, R. A. & Grandis, J. R. Targeting the IL-6/JAK/STAT3 signalling axis in cancer. *Nat. Rev. Clin. Oncol.* **15**, 234–248 (2018).
48. Yu, H., Lee, H., Herrmann, A., Buettner, R. & Jove, R. Revisiting STAT3 signalling in cancer: new and unexpected biological functions. *Nat. Rev. Cancer* **14**, 736–746 (2014).
49. Hailemichael, Y. et al. Interleukin-6 blockade abrogates immunotherapy toxicity and promotes tumor immunity. *Cancer Cell* **40**, 509–523.e506 (2022).
50. Harbour, S. N. et al. T(H)17 cells require ongoing classic IL-6 receptor signaling to retain transcriptional and functional identity. *Sci. Immunol.* **5**, https://doi.org/10.1126/sciimmunol.aaw2262 (2020).
51. Zhou, L. et al. IL-6 programs TH-17 cell differentiation by promoting sequential engagement of the IL-21 and IL-23 pathways. *Nat. Immunol.* **8**, 967–974 (2007).
52. Kimura, A. & Kishimoto, T. IL-6: regulator of Treg/Th17 balance. *Eur. J. Immunol.* **40**, 1830–1835 (2010).
53. Huseni, M. A. et al. CD8(+) T cell-intrinsic IL-6 signaling promotes resistance to anti-PD-L1 immunotherapy. *Cell Rep. Med.* **4**, 100878 (2023).
54. Liu, Y. et al. Tumor-repopulating cells induce PD-1 expression in CD8(+) T cells by transferring kynurenine and AhR activation. *Cancer Cell* **33**, 480–494.e487 (2018).
55. Bayik, D. & Lathia, J. D. Cancer stem cell-immune cell crosstalk in tumour progression. *Nat. Rev. Cancer* **21**, 526–536 (2021).
56. Clara, J. A., Monge, C., Yang, Y. & Takebe, N. Targeting signalling pathways and the immune microenvironment of cancer stem cells—a clinical update. *Nat. Rev. Clin. Oncol.* **17**, 204–232 (2020).
57. Bjørkøy, G. et al. p62/SQSTM1 forms protein aggregates degraded by autophagy and has a protective effect on huntingtin-induced cell death. *J. Cell Biol.* **171**, 603–614 (2005).
58. Johansen, T. & Lamark, T. Selective autophagy mediated by autophagic adapter proteins. *Autophagy* **7**, 279–296 (2011).
59. Wu, J. et al. Cyst(e)ine in nutrition formulation promotes colon cancer growth and chemoresistance by activating mTORC1 and scavenging ROS. *Signal Transduct. Target Ther.* **6**, 188 (2021).
60. Evavold, C. L. et al. Control of gasdermin D oligomerization and pyroptosis by the Ragulator-Rag-mTORC1 pathway. *Cell* **184**, 4495–4511.e4419 (2021).

61. Liu, Y. et al. Gasdermin E-mediated target cell pyroptosis by CAR T cells triggers cytokine release syndrome. *Sci. Immunol.* **5**, https://doi.org/10.1126/sciimmunol.aax7969 (2020).

Acknowledgements

This study was supported by grants from the National Natural Science Foundation of China (81930072, 82172870), Guangzhou Municipal Health Commission (No. 2023P-GX04), Cancer Innovative Research Program of Sun Yat-sen University Cancer Centre (CIRP-SYSUCC-0005), Overseas Expertise Introduction Project for Discipline Innovation (111 Project, B14035), Post-doctoral Innovation Talent Support Program (BX20200396), China Postdoctoral Science Foundation funded project (2021M693644).

Author contributions

X.-Y.L., J.M. W.-P.C. conceived the experiments. W.-P.C., Z.L., C.-Q.Z. and L.-F.L. carried out and analysed the data for most of the in vitro experiments. W.-P.C., Z.-M.X. and C.D. collected NPC samples and performed the IHC experiments. W.-P.C., J.-W.W., H.-M.W., Z.-J.D. and T.-X.H. designed and performed the animal experiments. X.-Y.L., W.-P.C., Z.L., C.-Q.Z. wrote and revised the manuscript. X.-Y.L., J.M., Y.-P.M. supervised the study. All authors reviewed and discussed the final version of the paper.

Competing interests

The authors declare no competing interests.

Additional information

Supplementary information The online version contains supplementary material available at https://doi.org/10.1038/s41467-025-62558-4.

Correspondence and requests for materials should be addressed to Yanping Mao, Jun Ma or Xiaoyu Liang.

Peer review information *Nature Communications* thanks Jonathan Schoenfeld, Nils Cordes, and the other, anonymous, reviewer(s) for their contribution to the peer review of this work. A peer review file is available.